Computational studies of structural properties of both CaO and CaS

A thesis presented

by

RAMUSI MATOME JACK

to

The Department of Physics

in fulfilment of the requirements

for the degree of

Master of science

in the subject of

Physics

University of Limpopo

South Africa, Limpopo province

Supervisor: P.E Ngoepe

Co-supervisor K.V Wright

[December] [2006]

Abstract

In this work, we are studying the properties of CaS and CaO structures in both atomistic simulation and Density Functional Theory. Defects formation (vacancies, impurity and interstitial) will be mechanism studied by using atomistic simulation method. In this approach, Mott-Littleton method will be used since it is a good approach of defects studies, and further explanation will be given on how the introduction of defects contribute on the stability of the bulk material. Diffusion of different atoms from one lattice site via interstitial path to vacancy lattice site, and how it segregates through the material, is also part of this study.

The surface properties will be studied using both methods mentioned. Surface energies calculations of different surface layers (e.g. CaS (100), CaS (110), CaS (111), CaO (100), CaO (110) and CaO (111)) is the approach we used to determine the most stable surface. In atomistic simulation, we further studied how percentage coverage of atoms contributes on the stability of the surfaces.

We further used Density Functional Theory to calculate surface energies of the above-mentioned surfaces. As in atomistic simulation method, we used surface energies to determine the most stable surface. In DFT we used only the most stable surface of both CaS and CaO to study the adsorption of molecules, namely H_2O, H_2S, HS and

S_2 on CaO (100) and CaS (100). The most/least-adsorbed molecule on both surfaces is explained in this study.

Declaration

I declare that the dissertation hereby submitted to the University of Limpopo for degree of Masters of Science has not been submitted by me or any other person for a degree at this or any university, and that the work herein is originally my own.

_____

Matome Ramusi Date 15 December 2006

Acknowledgments

I would like to thank various people and organizations who contributed in different ways to make this work a success. I highly appreciate and acknowlege the guidance and courageous support of Prof. P.E Ngoepe throughout the entire proccess of this work.

I would like to send my sincere gratitude to Prof K. Wright and C. R. A. Catlow for their guiding and stimulate discussion as well as valuable helpful input. All memberes of MMC and Royal Institution who contributed in various forms to making this work come through are greatly acknowleged.

The financial support from The National Reseach Foundation (NRF) of South Africa-The Royal Society (RS) of London collaboration and ESKOM is greatly acknowleged. The University of Limpopo for providing the state of art Materials Modelling Centre. (MMC), which is within the School of Physical and Minerals Science of Faculty of Heatlh, Sciences and Agriculture, with excellent facilities to enable us to perform all our calculations in this work.

Mostly, I am very much thankful to my family and friends who stood by me during difficult and challenging times and also for their patience throughout my period

of study. Lastly, I am greatful to everyone who might have contributed to the success of this work in one way or other.

Dedication

I dedicate this work to my parents, Maphari Ramusi (Mother) Maphala Ramusi (Father), Macheba Ramahlare (Grandmother), Tselahale Ramusi (Brother) Moloko Mogaila (Sister), My daughter (Motlatjo) and other members of the family who have supported me academically. I would like to thank them many times for having so positive contributed so that this work can come to real. Without them, I would not be where I am at the present moment.

KE A LEBOGA BATAU, KE ITUMELA KA THEKGO YEO LE ILEGO LA NTHEKGA KA YONA.

Content

List of Figures

Chapter 1
Introduction

Studies of lime (CaO) have been carried out some years ago. Most of these studies explained how the material contributes in the industries. CaO have been applied in varies industrial applications, e.g. ceramic, catalysis, painting. Portland cement is another area that we have identified so far, where CaO as one of the composition of cement play a major role in strengthening the product. Due to its high melting temperature it is likely to find more industrial applications with the advance of high temperature technology. The diffusion parameters that mostly occur at high temperature became one of the interesting goals that have paid attention in CaO studies [1, 2, 3]. Since it is applied in different ways, it became one of the materials that are studied both experimentally [2, 3] and through computational studies [4]. CaO has been investigated and it was realized that CaO (100) surface is more reactive with water molecules [1]. The adsorptions of water molecules on the surface also play a vital role in the adsorption process. The adsorptions of water molecules were investigated on different surface layers of CaO and MgO. Both mentioned (CaO and MgO) materials have similar structures that are expected to follow the same trends in other structural parameters, e.g. the stability of the surface layers [4] and the adsorption of molecules. From the information we have aquired so far it shows that CaO became one of the minerals that play a major role in industrial applications. We have noted, from most of the literature, how frequently this material was cited.

In recent studies, there are many goals in which researchers were interested in, because of its many applications. Some researchers focused on the catalytic behaviour of the material [5], where CaO and Carbon catalysis, were mixed with each other in chemical bonded states. And other research focused on its properties as a coating agent due to its high melting temperature. Dolomite as one of the materials that contains higher percentage of CaO has been used as a coating agent of pellets for sticking prevention in order to optimised the blast furnace operation [5].

1.1 Overview of computational and how it relate with experimental and theory.

Computer technology, particularly in the areas of increased speed of calculations and more efficient memory storage devices, has improved at a rapid pace over the past 20 years. Many of the improvements in computer hardware and in the algorithms (software) that control computers have presented a new tool for investigating scientific problems. Scientific research can be categorized in three areas: observational science, experimental science and theoretical science.

A fourth and new area of scientific research has emerged over the past 40 or 50 years that is revolutionizing how scientists work and how they think about doing science. Computational studies are the application of computational and numerical techniques to solve large and complex problems. It takes advantage of not only the improvements in computer hardware, but probably more importantly, the improve-

ments in computer algorithms and mathematical techniques. Computational studies allow us to do things that were previously too difficult to do due to the complexity of the mathematics, the large number of calculations involved, or a combination of the two. Computational studies also allows us to build models that help us to make predictions of what might happen in the laboratory, so that we are perhaps better prepared to make good observations or to understand better what we are seeing. We can also use computational studies methods to perform experiments that might be too expensive or too dangerous to do in the laboratory. We can, for example, use computational techniques to design various parts of the automotive industries in shorter cycles. This also assists in battery material to come with clear prediction of best material that will extend the life time of the rechargeable batteries. While computational models cannot replace the laboratory, they have certainly become an intricate part of the overall search for scientific knowledge.

We consider computational studies to be a fourth method of doing research, an addition to observational, experimental, and theoretical methods:

Figure 1.1, shows that science is defined as the study of how nature behaves. The three supporting sciences are theoretical, experimental, and computational. There is clearly a "symbiotic" relationship between the three – theoretical findings "drive" the experimentalists, experimental data is used to build and validate computational research, computational research provides the theorists with new directions and ideas. Many of the fundamental questions in science (especially those with potentially

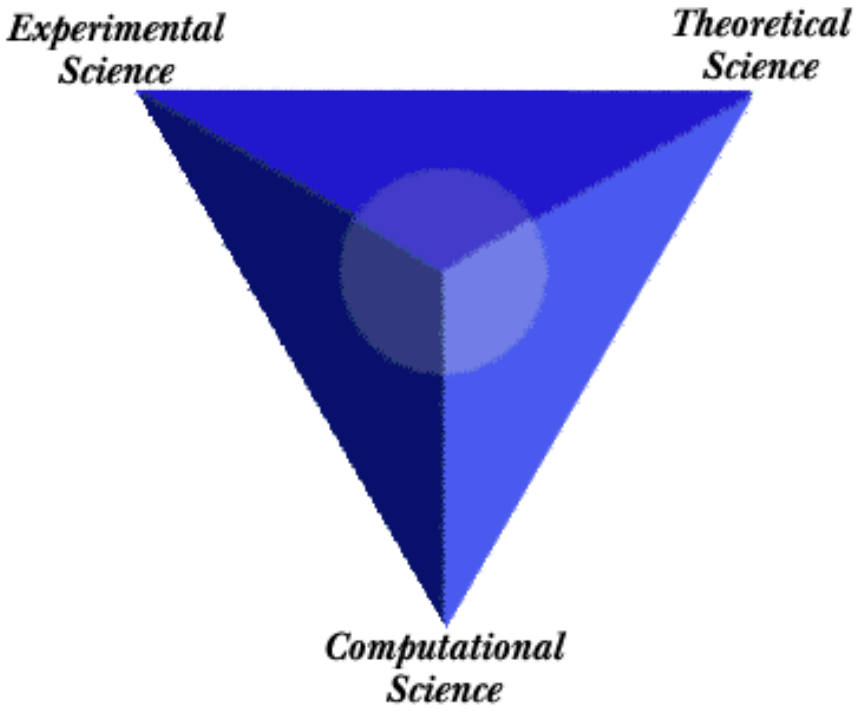

Figure 1.1: The study of how nature behaves[6]

Minerals name	% of CaO[7]
Limestone	54.89
dolomite	34.37

Table 1.1: Content of CaO in Chichibu limestone.

broad social, political, and scientific impact) are sometimes referred to as "Grand Challenge" problems. Many of the Grand Challenge problems are those that can only be solved computationally. Certain research problems in science, are considered by all computational simulation studies to be one of the major grand challenge categories. In material research, the argument has been made that we have known, since 1928, all of the theoretical science needed to solve every chemical problem. It is only since the birth of computational science (late 1950's) that we had the tools and technologies needed to solve these complex mathematical equations born from the theorists. There are other ways of looking at computational sciences. Some will describe it as the intersection of three disciplines: We use a slightly different, less discipline-specific picture of computational science: application, algorithm, and architecture:

1.2 Background information of CaO and other Industrial applications

CaO is produced from limestone ($CaCO_3$), through heating [8]. When we investigate application of limestone and dolomite, we realize that chemical proccess of the material became successfull because CaO is one of the composition in the materials as

Figure 1.2: The sample of limestone that contains the composition of some minerals

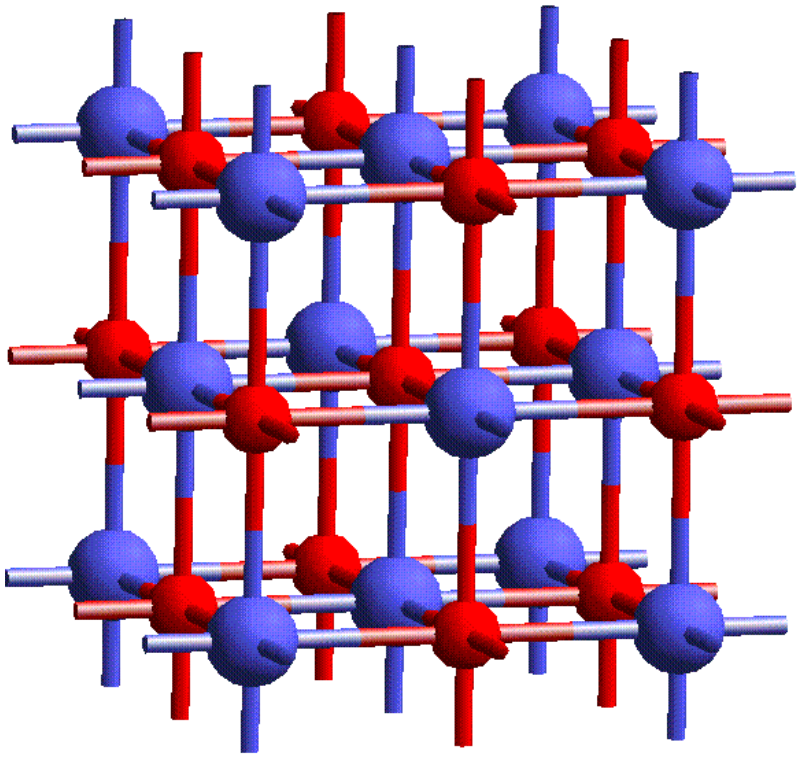

Figure 1.3: The structure of CaO

shown in Table 1.1. The material composition depends on the type of the mineral and the geographical origin of the material. The content of CaO in limestone as shown in figure 1.2 is estimated at 54.89%, and 34.37% of dolomite [7].

Many metal halides and oxides crystallizing in the cubic rock salt structure, tend to be highly ionically bonded. Large anions are arranged in cubic close packing and all the octahedral interstitial positions are filled with cations in the structure shown in figure 1.3. CaO has a rock salt structure with space group Fm-3m, and the positions are allocated as follows: O atoms at [0.5;0.5;0.5] and Ca at [0,0,0] positions. The lattice parameter of this cubic structure is a = 4.805Å.

CaO is a white crystalline solid with a melting point of 2572°C and its density is 3340kg/m^3. It is manufactured by heating limestone, coral, sea shells, or chalk, which are mainly $CaCO_3$, to drive off carbon dioxide as follows:

$$CaCO_3(s) = CaO(s) + CO_2$$

The reaction is driven to the right by flushing CO_2 from the mixture as it is released. The production of CaO from limestone is one of the oldest chemical transformations produced by man. The abundance of limestone in the Earth's crust and the ease of its transformation to CaO do not alone explain why the lime is one of the oldest products of chemistry. Lime has many properties that make it quite valuable. It is so useful, that it is today produced industrially on a vast scale.

1.2.1 CaO is also used to coat the interior the stainless steel walls of power generation boilers.

Calcium oxide is a possible coating material because it is an excellent electrical insulator and it has large negative free energy to prevent the the reaction with liquid lithium because of its high heat resistivity [9]. It was proven scientifically that coated material has longer lifetime periods and also improved performance by reducing the thermal conductivity of the material [10]. CaO/lime as coating agents reduce moisture penetration and improves resistance against sulphur reaction with the boiler [11].

Owing to its capability, CaO can act as a protecting agent of some gases (sulphur compund gases) that are emitted from coal during the combustion process. A by-product from one of the industries e.g. New Zealand Dairy Corporation factory,

fluidized bed boiler ash contains economically useful amounts of lime and sulphur. The fluidized bed boiler is produced from injection of limestone into the combustion chamber to absorb and reduce SO_2 and the other sulphur compounds emitted from burning high sulphur-rich coal [12]. Some of the emitted gases, mentioned earlier, are CO_2 and H_2S. During the burning process CaO reacts with CO_2 at a higher pressure and temperature to form $CaCO_3$. During the process CO_2 and H_2S will react with CaO from the walls of the boilers, as results $CaCO_3$, CaS and H_2O will be formed.

1.3 Rationale of this study

Most of CaO originates from limestone and dolomites through chemical reactions. This material has high melting temperature that has good industrial applications. Owing to its high melting temperature, some of its applications involve coating boilers that are always experiencing high temperatures during combustion. In addtion to coating, CaO has catalytic properties that are valuable during certain chemical reactions in the laboratory. It has high resistivity and is used also in the production of ceramic materials. In the laboratory, the material has been tested to adsorb some chemicals, e.g. water, sulphur compounds etc.

1.4 Motivation of the dissertation

CaO is one of the materials used in many industrial applications, including those needing high heat resistance. At power utility industries such as Eskom's, coal is used to generate electricity. Since CaO has a high melting temperature, it has been used to coat the interior walls of boilers with an aim of protecting them from corrosion caused by the sulphur compound emitted from the sulphur-rich coal used during the combustion process. Even though CaO is useful as a coating in boilers, it was noted that some sulphur compounds could diffuse through CaO and form a layer between CaO and the metal wall of the boiler.

In the current work, we have studied the bulk and surface properties of CaO and CaS. The main objective is to study the mechanisms reponsible for the corrosion of metal walls of boilers and to suggest possible ways of avoiding this problem. CaS material is included in this study because during the reaction of sulphur and CaO on the walls of the boiler, CaS is formed.

1.5 Outline of the dissertation

The dissertation is arranged as follows

Chapter one gives the background information on computational, experimental and the theoretical aspects of CaS and CaO systems.

Chapter two outlines computational methods used in this study.

Chapter three gives structural properties of the systems. In this chapter attention is focused on the predictions of structural parameters. This includes how the systems are being set, e.g. cut-off energy, k-points mesh, and the lattice parameter variation in both CaS and CaO systems. The validation of new potentials will be discussed.

Chapter four is on results calculated by atomistic simulation. In this chapter, we will explain the defect formation on both CaO and CaS systems; diffusion of atoms on the interstitial path in both systems will be discussed. The impact made by foreign atoms on the surfaces will also be discussed.

Chapter five presents the Density Functional Theory results, and in particular the adsorption of the molecules, H_2O, HS, S_2 and H_2S on both CaO (100) and CaS (100) surfaces.

Chapter six contains the summary and conclusion and also recommended future work.

Chapter 2
Background of computational methodology and methods of calculation in the current study

The advent of quantum mechanics opened the door to understand the fundamental interaction of the atomistic constituents of matter and turn to use this knowledge to design and control material properties and processing. In practice, the solution of the quantum mechanics equation is intractable, except in relatively simple cases. Therefore the control of the material structure at various length scales has necessarily progressed by intuition and by trial and error in the laboratory. This time the approach is not about to be replaced, but in many laboratory it is being supplemented by computer aided research and development. Today most of pharmaceutical companies' routine seeks insight and guideline in the design of new drugs using computer simulation of molecular interaction [13]. Similarly at the macroscale, companies such as Boeing and Ford supercomputers are used to model airflow and other characteristic of design features before they actually build model for testing in wind tunnel of crashing into walls. It is much cheaper to design on the computer.

The thousand fold increases in computational power, resulting from new machines with massively parallel architecture, promise to change, dramatically, the use of computational simulations in helping materials research. Computing power is about to reach the level at which we can finally solve the quantum mechanical equa-

tions for large enough systems and elucidate complex atomistic interaction occurring over length scale involving thousand of atoms. Scientists can envision a path that allows accurate simulation starting at atomistic and proceeding to an intermediate length scale where many of the bulk material properties, such as strength, are determined. Results from simulation at the intermediate length scale will naturally feed into continuum model to simulate the macroscopic engineering designs. The idea of accurate simulation capabilities at each of the length scales together with the possibility of overlapping the length is empowering.

A primary goal of a material simulation initiative would be to develop a capacity to reliably predict the properties of real material. To achieve this goal one must be able to realistically simulate physical phenomenon over a vast range of time and length scales. For example, there is currently incomplete understanding of how the underlying structure defects impact on the mechanical properties of real material. Some of the mathematical methods used to model material physics are generally empirically based with phenomenological parameters. One important challenge is to determine these parameters entirely from first principle calculations.

There is different classification of characteristic range of time and length scale appropriate to materials. It is necessary to uncover the elusive connection in hierarchy of quantum/molecular, atomistic/nano, macroscopic and macroscopic scale and to unravel the complex of the interactions that govern the properties and performance of

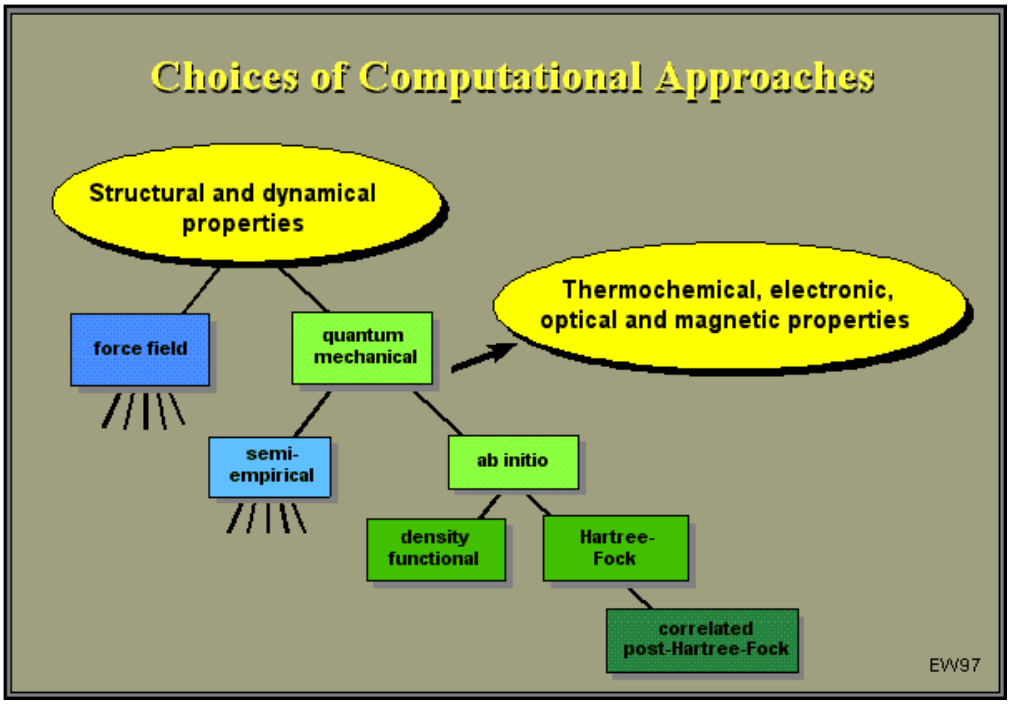

Figure 2.1: Choice of computational method[14]

material. In the next section we will discuss the different appraches of computational modelling, in particular ab intio and atomistic simulation.

2.1 Choice of methods

Figure 2.1 shows major choices of computational approaches for the simulation and prediction of structural and functional properties. For structural and dynamical propeties investigations, two computational methods are suggested quantum mechanical and force field. If structural and energetic questions need to be answered, which is often the case in the first stage of modelling and simulation of materials, force field meth-

ods are preferable because of the high computational efficiency. However, one needs to be aware that the generality and transferability of force fields cannot be taken for granted and the results obtained from force field calculations can be misleading.

Among quantum mechanical methods, the next choice is between ab initio and semiempirical approaches. The latter approach is preferable (semi empirical) because of the less amount of computational speed required in the calculations. However, as with force field methods, semiempirical methods should be used with great care since the range of applicability of the inherent approximations and parameters needs to be controlled. Ab initio method typically provide reliable results, but the sensitivity of the results on the choice of computational parameters, in particular the choice of the basis functions and the level of correlation requires attention.the next choice is between DFT and Hartree- Fock method.

Experience so far has shown that DFT method tend to be more robust than Hartree-Fock method in the sense that with a reasonable choice of basis functions and other computational parameters, the geometric structures, the vibrational frequencies, and the electronic structure obtained from DFT calculations usually do not give strong and unexpected deviations from experiment, while this may be the case with Hartree-Fock calculations for systems where a single determinant is not appropriate (which may not be a priori obvious to the non-expert) [15]. Correlated post-Hartree-Fock methods such as coupled-cluster theory are very time consuming and require a careful control of the computational parameters such as basis functions.

This level of computation is possible only for rather small systems and the relevance to the actual materials design problem might thus be questionable, despite the high accuracy of the results.

As hinted in Figure 2.1, there are many possible choices within semi empirical and force field methods, which are linked to the availability or applicability of parameters. This is not the case with ab initio methods. In fact, the amount of computational time possible to run a Hartree-Fock calculation is actually quite limited. For example, only Gaussian-type basis sets are practical and the computational task is reduced to the evaluation of analytic expressions. This is not the case for density functional calculations, where the greater formal simplicity of the Hamiltonian enables greater freedom in the choices of algorithmic implementations. DFT and atomistic simulation will be considered in this current work.

2.2 Method of calculation used in the current work

Computer simulation, also known as computer modelling, is the use of computers to develop and explore numerical models that reproduce the properties of natural and/or synthetic materials. Atomic-level computer simulation involves basing these models on the individual atoms and molecules (and sometimes electrons) that make up the material. The methods used range from rigorous (and computational expensive) treatments derived from Schrödinger's equation, referred to as ab initio quantum mechanical methods in this chapter to rapid empirical techniques which use approximate

functions to describe the forces between particles. The method chosen for any particular problem depends on the size of the system, the type of bonding in the material (ionic, covalent, etc), and the kind of information desired.

2.3 Atomistic simulation

An atomistic simulation technique is a forcefield method involves potentials parameters is knows as semi empirical or empirical method. For empirical method, we apply only derived potentials, and for semi empirical we used the experimental potentials and fit them in computer to simulate the systems for investigations of structural properties.

2.3.1 The interatomic potential

The best choice of a potential for simulations depends on how best it can reproduce the structural parameter. There is a variety of potentials that can be used to model different systems, e.g. Lennnard – Jones potential, Buckingham potentials, Morse potentials and etc.

This set of potentials have their own speciality accounting to the given task on the type of systems, e.g. Lennard – Jones potential (L.J) does not give adequate description of all the properties of metals. This relation is proved to be wrong for most of the metals. Pair-wise potentials fail to estimate the structure relaxation and reconstruction around point defects (vacancies and self-interstitials) in metals. The

vacancy formation energy obtained by means of pair - wise potentials is overestimated, and is found to be about equal to the bulk cohesive energy.

The solution of the problem is an introduction of a many-body potential, which include a pair-wise interactions only as part of the full potential. This first part of the many-body potential accounts for the core - core interactions (or ion - ion interactions), while the second part incorporates the complex nature of metallic cohesion by an additional term:

$$\mathbf{U} = \mathbf{U}_1 + \mathbf{U}_2\boldsymbol{\rho}(\mathbf{r})] = \frac{1}{2}\sum_{i:i\neq 1}^{N} \boldsymbol{\phi}(\mathbf{r}_{ij}) + \frac{1}{2}\sum_{i=1}^{N} \mathbf{U}(\mathbf{n}_i) \tag{2.1}$$

Where the $\phi(r)$ is the two-body part, and the many-body part U(n_i) depends on electronic charge density around the atom i:

$$\mathbf{n}_i = \sum_{i\neq j}^{N_g} \boldsymbol{\rho}(\mathbf{r}_{ij}) \tag{2.2}$$

Where N_g is the number of nearest neighbours of the atom i.

2.3.2 Coulomb interaction

When considering ionic materials, the Coulomb interaction is by far the dominant term and can represent, typically, up to 90% of the total energy. Despite having the simpliest form, given by Coulomb's law;

$$U_{ij} = \frac{q_i q_j}{4\pi\varepsilon_0 r_{ij}} \tag{2.3}$$

it is in fact the most complex to evaluate for periodic systems. This is because the Coulomb energy is given by a conditionally convergent series, i.e. the Coulomb

energy is ill-defined for an infinite 3-D material unless certain additional conditions are specified. The reason for this can be readily understood - the interaction between ions decays as the inverse power of r, but the number of interacting ions increases with the surface area of a sphere, which is given by $4\pi\varepsilon_0 m^2$. Hence, the energy density of interaction increases with distance, rather than decaying. One solution to the problem, proposed by Evjen [16], is to sum over charge-neutral groups of atoms. However, by far the most widely employed approach is the method of Ewald [17] for three-dimensional materials. Here the conditions of charge neutrality and zero dipole moment are imposed to yield a convergent series with a well-defined limit. To accelerate the evaluation, the Coulomb term is subjected to a Laplace transformation and then separated into two components, one of which is rapidly convergent in real space, and a second which decays quickly in reciprocal space. Conceptually, this approach can be viewed as adding and subtracting a Gaussian charge distribution centred about each ion [18]. The resulting expressions for real and reciprocal space, as well as the self-energy of the ion, are given below:

$$U^{\text{real}} = \frac{1}{2}\sum_{i=1}^{N}\sum_{j=1}^{N}\frac{q_i q_j}{r_{ij}} efrc(\eta^{\frac{1}{2}} r_{ij}) \tag{2.4}$$

$$U^{recip} = \frac{1}{2}\sum_{i=1}^{N}\sum_{j=1}^{N}\sum_{G}\frac{4\pi}{V} q_i q_j \exp(iGr_{ij})\frac{\exp(-\frac{G^2}{4\eta}}{G^2} \tag{2.5}$$

$$U^{self} = -\sum_{i=1}^{N} q_i^2 \left(\frac{\eta}{\pi}\right)^{\frac{1}{2}} \tag{2.6}$$

$$U^{electrostatic} = U^{\text{real}} + U^{recip} + U^{self} \tag{2.7}$$

Here *q* is the charge on an ion, *G* is a reciprocal lattice vector (where the special case *G* = 0 is excluded),*V* is the volume of the unit cell, and η is a parameter that controls the division of work between real and reciprocal space. It should also be noted that although the reciprocal space term is written as a two-body interaction over pairs of atoms, it can be rewritten as a single sum over ions for more efficient evaluation. The above still leaves open the choice of cut-off radii for real and reciprocal space. One approach to defining these in a consistent fashion is to minimise the total number of terms to be evaluated in both series for a given specified accuracy, [19]. This leads to the following expressions:

$$\eta_{opt} = \left(\frac{N\omega\pi^3}{V}\right)^{\frac{1}{2}} \tag{2.8}$$

$$r_{\max} = \left(\frac{\ln(A)}{\eta}\right)^{\frac{1}{2}} \tag{2.9}$$

$$G_{\max} = 2\eta^{\frac{1}{2}}(-\ln(A))^{\frac{1}{2}} \tag{2.10}$$

Note that the above expressions contain one difference from the original derivation, in that a weight parameter, has been included that represents the relative computational expense of calculating a term in real and reciprocal space. Tuning of this parameter can lead to significant benefits for large systems. There has been several modifications proposed for the basic Ewald summation that accelerate its evaluation

for large systems, most notably the particle-mesh [20], and fast multipole methods [21]. Furthermore, there are competitive approaches that operate purely in real space for large unit cells and that scale linearly with increasing size, such as the hierarchical fast multipole methods, though care must be taken to obtain the same limiting result by imposing the zero dipole requirement. The latter approach can also be applied to accelerating the calculation of the Coulomb energy of finite clusters.

In principle, it is possible to calculate the Coulomb energy of a system with a net dipole, μ, as well. The nature of the correction to the Ewald energy can be determined as a function of the shape of the crystal, and the formula below can also be employed [22]:

$$U^{dipole} = \frac{2\pi}{3V}\mu^2 \tag{2.11}$$

However, the complexity of using the above correction is that it depends on the macroscopic dipole of the crystal, and even on any compensating electric field due to the environment surrounding the particle. Hence the dipole moment is usually ill-defined, since it depends on the surfaces, as well as the bulk material. Even if we neglect surface effects, the definition of the dipole moment is ambiguous since the operator is not invariant under translation of atomic images by a lattice vector. Consequently, we will take the Ewald result as being definitive.

Similarly, it is possible to relax the charge neutrality constrain, and to perform calculations on charged supercells [23], provided care is taken when constructing thermodynamic cycles. This is often used when probing defect energetics as an al-

ternative to the Mott-Littleton method. Here the net charge, *Q* is neutralised by a uniform background charge, leading to an energy correction of:

$$U^{backround} = \frac{\pi}{2V\eta}Q^2 \tag{2.12}$$

So far we have only considered how to handle infinite 3-D solids, but the same issues exist for lower dimensionalities.

2.3.3 Short-range potential function

Two body-potentials represents short-range interaction between two charge clouds, and can be attractive (Van der Waals) or repulsive. The interaction has various analytical forms and depends on the type of the system being modelled. However all the analytical forms can be classified under bonded and non-bonded interactions. A number of these forms will be describes in the next sections (2.3.4 - 2.3.7).

2.3.4 Harmonic potential function

Modelling interaction between bonded ions can be achieved using harmonic potential form, which its analytical form is written as

$$U(r_{ij}) = \frac{1}{2}k_{ij}(r_{ij} - r_o)^2 \tag{2.13}$$

where the parameter K_{ij} represents the force constant associated with the derivation from the equilibrium bond separated and r_0 the equilibrium bond separation. This potential is harmonic due to energy being dependent on the square of the displacement of the current bond length (r_{ij}) from the equilibrium bond length, and is

used only when the bond length does not vary much from the equilibrium position. For interactions where the bond stretching are large, Morse potential is discussed in section 2.3.5.

2.3.5 Morse potential function

Morse potential is used for covalent bonding when distance vary from the equilibrium bond distance at it displays the correct harmonic behaviour missing from the harmonic function. It is thus able to model systems away from their equilibrium bond distance such as point defect and surfaces or when temperature or pressure is applie, and takes the form:

$$U(r_{ij}) = A_{ij}\left\{1 - \exp\left[-B_{ij}(r_{ij} - r0)\right]\right\} - A_{ij} \tag{2.14}$$

where A_{ij} is the bond dissociation energy, r_0 is the equilibrium bond distance and B_{ij} is the function of the slope of the potential energy well and can be obtained from spectroscopic data; due to its inclusion of the bond energy the Morse potential is often used with subtraction of the Coulomb interaction, allowing it to complete by describing the bond for nearest neighbours. For second nearest neighbours a non-bonded potential, such as Buckingham and Lennard ones can be used and are described below in section 2.3.6 and 2.3.7.

2.3.6 Buckingham potential form

The Buckingham potential form is the most widely used to model non-bonded interactions. It contains a repulsion and attractive term and takes the form:

$$U(r_{ij}) = A_{ij} \exp\left(\frac{-r_{ij}}{\rho_{ij}}\right) - \frac{C_{ij}}{r_{ij}^6}[24] \tag{2.15}$$

where the A_{ij} is associated with the hardness of the ions, $\boldsymbol{\rho}_{ij}$ is related to the size of the ions and C_{ij} is the term included to model dispersion.

2.3.7 Lennard-Jones potential form

Lennard-Jones potential has a form of nonbonded interaction with a repulsive part dependant on r^{-12} and attractive part depend on r^{-6} as in the Buckingham case, and is given by:

$$U(r_{ij}) = \frac{A_{ij}}{r_{ij}^{12}} - \frac{B_{ij}}{r_{ij}^6} \tag{2.16}$$

This potential also used for modelling noble gas lattice interactions for interaction between polar and non-polar materials.

2.3.8 Shell model

In atomic physics, the shell model proved successful in providing an explanation for the detail of atomic structure. Atomic shells were filled with electrons in order of increasing energy subject to Pauli exclusion principle. As a result of the success of the atomic shell model, this model was extended to the real nuclei.

The shell model also known as independent model, treats the nucleons individually as opposed to treating the nucleus as a whole. The long range repulsive coulomb force and the short-range attractive nuclear force interaction between nucleons are replaced by an average force. The shell model describe the nucleons in terms of groups or shells, with the position and energy of a nucleons depends upon its quantum numbers.

There were however, several principle that needed reworking, compared with atomistic structure. In atomistic structure the potential is provided by the Coulomb fieled of the nucleus, whereas in the nuclear case the motion of a single nucleon is governed by an average potential generated by all the other nucleons. If two nucleons collide, the energy required to excite one of them to higher-lying orbit would be more than the nucleons are likely to transfer. Therefore, in the nuclear case, it is assumed that there are no nucleon-nucleon collisions and each nucleon moves in an unperturbed single particle orbit within the nucleus.

In shell model, atomistic interactions are represented by potentials between each pair of atoms in the system. Electron polarization of the atoms is implemented via the Dick overhauser model [25], in which an atom is considered as a charge core connected by a harmonic spring to a massless charge shell. The equilibrium distance between the core and shell is representation of the electric polarization of that atom. This is important as there are no electrons in the shell model, all atoms

are effectively represented by point charge and the shell approximates the effective of electron density flow on the atomic interaction.

The interaction between core and shell is controlled by empirical potentials whose parameters are fitted to archive the best possible comparison with experimental or computational techniques. The potentials are usually derived from three interactions electrostatic coulomb interactions between the atoms, van der waals interactions and short-range repulsive interactions. The charge-charge electrostatic interaction between atoms *i* and *j* given as the sum of four terms:

$$V_i^{elec} = \sum_j^n \frac{q_i q_j}{4\pi\varepsilon_0 |r\delta_i - r\delta_j|} + \sum_j^n \frac{Q_i Q_j}{4\pi\varepsilon_0 |r\zeta_i - r\zeta_j|} + \sum_j^n \frac{Q_i q_j}{4\pi\varepsilon_0 |r\zeta_i - r\delta_j|} + \sum_j^n \frac{q_i Q_j}{4\pi\varepsilon_0 |r\delta_i - r\zeta_j|} \tag{2.17}$$

Where $i \neq j$, n is the number of atoms q_i is the shell charge of atoms *i*, Q_i is the core charge of atom *i*, $r\delta_i$ is the position vector of the shell of atoms *i*, and $r\zeta_i$ is the position vector of the core of atoms *i*. Buckingham potentials (two body terms) were the potentials behind this interaction to represent the non-coulombs short-range interaction between the shells. These potentials have the following form:

$$V_i^{short} = \sum_j^n -C|r\delta_i - r\delta_j| - 6 + Ae^{-\frac{r\delta_i - r\delta_j}{\rho}} \tag{2.18}$$

Where C, A and ρ are parametrized constant specific to each pair of shell *i* and *j*, and $i \neq j$. The first term in the equation 2.18 represent the attactive van der Waals interaction and the second term the short-range repulsion due to electron clouds over-

lap. For shell there is also an additional contribution to the interaction due to the elastic force in the spring connecting core and shell. This force is equal to kδr*i*, where k is the polarized spring constant between the centre of core and shell for atom *i.* The spring interaction between the shells is given by:

$$V_i^{spring} = \frac{1}{2} k \delta r_i^2 \tag{2.19}$$

Combining equations (2.17),(2.18) and (2.19) gives the total energy of the system as:

$$E = \frac{1}{2} \sum_{j}^{n} \left[V_i^{elec} + V_i^{short} + 2V_i^{spring} \right] \tag{2.20}$$

This can be minimised with respect to core and shell position to find the equilibrium geometry of relaxed atoms in the system. Usually certain atoms within the tip-surface unit cell remain frozen to represent the interface between the macroscopic and microscopic fature (Refer to Mott-Littleton method in section 2.3.10 for futher explanation)

2.3.9 Modelling point defects

There are two widely used approaches of calculating defects. There is embedded cluster [28] and supercell technique. The embedded cluster method is too ideal for infinite dilute limit and the supercell method is appropriate for very large bulk systems

concentration of defects where there exits defect-defect interaction. This supercell method is mainly applied in large bulk systems.

2.3.10 Supercell method

The supercell method is one of the defect calculation methods that work better in large periodic system. The supercell containing defects is repeated periodically throughout space and depends on the size of the supercell e.g. 2x2x2, 3x3x 3 etc. The key quantity of calculating the defects formation energy in the system is given by the equation:

$$E_d^C = E_T^C(defect^q) - E_T^C(no-defect) + \sum_i \mu_i n_j - q(\varepsilon_v + \varepsilon_f) \qquad (2.21)$$

where $\mathbf{E}_T^C$ (defect) and $\mathbf{E}_T^C$ (no-defect) are the total energy of the supercell "C" with and without defect. The defects is formed by adding/removing $\mathbf{n}_i$ atoms of chemical potential μ_i. ε_f is the Fermi level, measuring from ε_V the valence band edge. Almost all properties of defects can be derived from variations in and differences between formation energies. The method is very powerfull, but critical limitations remain. Two of the most important being the relative small number of atoms which can be treated and the effect of the approximations, such as LDA and GGA required to solve the DFT itself.

Figure 2.2: The two region approach to calculate defect energies, where the inner black sphere represents a defects, the orange sphere represents the boundary of region I, the grey sphere region IIa , while region IIb tends to infinity [26].

2.3.11 Embedded cluster method

Figure 2.2, explains cluster technique method referred as Mott-Littleton method. This is a point defects approach which is based on the idea that total energy of the trace- element bearing system is minimised by a relaxation of the position of the atoms surrounding the element, and divided the crystal into regions as shown in figure 2.2, the crystal is divided into an inner region I (inner black) immediatelty surroundeding the point defect, where the relaxation is assumed to be the greatest, and an outer region (II), which is only slightly pertubed. In the inner region the elastic equation for the force are solved explicitly to dertermine the relaxations, and in the outer region these are estimated using Mott-Littleton approximation [27]. These is normally also an interface region IIa (grey) surrounding the inner region.

Within the two region approach, the total energy of the system, U, is given by

$$U(x,y) = U_1(x) + U_2(x,y) + U_3(y)[28] \tag{2.22}$$

where x and y label the coordinates of the ions in the inner region I and the displacement in the outer region II, respectively. U_1 and U_3 arises solely from interaction within each region, while U_2 is the interaction energy between them. In this case we assume that for region II the effect of the force is very small in such a way that the region will be purely harmonic. Assuming that U_3 is a quadratic function of y, then together with the equilibrium condition states as:

$$\frac{\partial U}{\partial y} = 0 \tag{2.23}$$

can be written in terms of the derivatives of U_2 and so an expression for U is obtained in which the the explicit dependence of the total defect energy on U_3 has been removed. In this case we assume that for region II the effect of the force is very small in such away that the region will be purely harmonic.

Then the total energy of the region two can be written as:

$$U_3(y) = \frac{1}{2} y^T H_3 y \tag{2.24}$$

where H_3 is the Hessian matrix for region II.

Now for the equilibrium displacement of region II then the total energy of the whole system is given by:

$$\left(\frac{\partial U_{tot}(x,y)}{\partial y}\right)_x = \left(\frac{\partial U_2(x,y)}{\partial y}\right)_x + H_3 y = 0 \tag{2.25}$$

therefore

Then combining equations 2.24 and 2.25 with the previous one we get

$$U_2 = -\frac{1}{2}y \tag{2.26}$$

Then the total energy of the system becomes

$$U_{tot}(x,y) = U(x)_1 + U(x,y)_2 - \left(\frac{\partial U_2(x,y)}{\partial y}\right)_x y \tag{2.27}$$

Then the problem of calculating the defects due to region one and region two is given by

$$U_{defect}(x,y) = U_{tot}(x,y) - U_{tot}(x,y) \tag{2.28}$$

2.4 Ab initio method

The term ab initio means from first principles. It does not mean that we are solving the Schrödinger equation exactly. It means that we are selecting a method that in principle can lead to a reasonable approximation to the solution of the Schrödinger equation and then selecting a basis set that will implement that method in a reasonable way.

By reasonable, we mean that the results are adequate for the application in hand. A method and basis set that is quite adequate for one application may be totally inadequate for another application. We also have to take into account the cost of doing calculations and the total amount of computer time required. If an answer is needed today, there is no point in doing a calculation that will take long time of with

the results coming back after many days. However, if the results are not adequate for the purpose, there is no point in doing the calculation, however cheap it may be.

A wide range of ab initio methods have been employed, but we will restrict ourselves to the sub class of methods that is employed in the vast majority of all calculations carried out within a short reasonable short time. This is the sub class that uses the molecular orbital method, possibly followed by a post molecular orbital method that uses the molecular orbital wave function as the reference function. The molecular orbital method is generally referred to as the Hartree-Fock method. This theory will be discussed on the following subsection 2.4.1.

2.4.1 Hartree Fock method

The Hartree-Fock method is based on approximation that each electron moves in the average potential from the nucleus and the other electrons. This assumption leads to the independent-particle model, which essentially reduce the many-electron problem to the problem of solving a number of coupled single-particle equations.

The single-particle equations are solved in an iterative way which will be described below. Hartree made the first calculation based on these ideas already 1928 [29], but calculations of this type are of course best suited for computers. Today there are several computer codes available for anyone who is interested in atomic properties.

The Hartree-Fock approximation is a fast and reliable method for a wide range of atomic systems, but it is just a first approximation. Nowadays there are several calculation schemes developed which can produce much more accurate results. For systems with few electrons, as helium, the "many-body problem" can be solved more or less exactly

General many-electron systems cannot be treated with such a precision, but a large part of the electron correlation, i.e. effects beyond the independent particle model, can be accounted for with methods such as configuration interaction or perturbation theory.

'Ab-initio' is a term used to describe an accurate solution of the non-relativistic, time independent Schrödinger equation[30]

$$H\psi = E\psi \tag{2.29}$$

Where, H is the Hamiltonian operator for the system, a function of kinetic and potential energies of the particles of the system, ψ is the total molecular wavefunction, and E is the molecular energy.

For most of the system can't do it analytically to solve this equation for anything other than the hydrogen atom. For this reason, for a many body system, approximations are introduced to simplify the calculations. One of these approximations is that of Born and Oppenheimer where the approximation that as the electrons travel much faster than the nuclei, the electrons can be assumed to be travelling in a po-

tential generated by a stationary nucleus. This approximation allows the electronic Hamiltonian to be considered for a fixed set of nuclear co-ordinates.

$$\mathbf{H}_{elec}=\sum_{i=1}^{n}-\frac{h^2}{8\pi^2 m}\bigtriangledown_i^2-\sum_{i=1}^{n}\sum_{a=1}^{N}\frac{Z\alpha e^2}{4\pi\epsilon_0 r_{i\alpha}}+\sum_{i}\sum_{\angle j}^{n}\frac{^2}{4\pi\epsilon_0 r_{ij}} \tag{2.30}$$

In equation above the first term contributing to the electronic Hamiltonian is the electronic kinetic energy where *n* is the number of electrons, the second, the electron-nuclear attraction energy and the third, electron-electron repulsion. The equation can be greatly simplified by working in atomic units, where electron charge (e) and mass (m) are defined as unity. The equation then becomes,

$$\mathbf{H}_{elec}=\sum_{i=1}^{n}-\frac{1}{2}\bigtriangledown_i^2-\sum_{i=1}^{n}\sum_{a=1}^{N}\frac{Z_\alpha}{r_i}+\sum_{i}\sum_{\angle j}^{n}\frac{1}{r_{ij}} \tag{2.31}$$

Another approximation is the description of the wavefunction in terms of the one electron functions, i.e. orbitals. This approximation gives the Hartree product

2.4.2 Density Functional Theory

In density functional theory (DFT), The total energy of the system, E_{total} defined as a function of ρ, the charge density.

$$E_{total} = T[\rho] + U[\rho] + E_{xc}[\rho] \tag{2.32}$$

Where T[ρ]is the kinetic energy of a system of non-interacting particles of density ρ, U[ρ] the classical Coulomb energy and E_{xc}[ρ] is a term containing exchange

and correlation. Again, an iterative procedure is used to evaluate the equation by varying ρ until self consistent. Whilst equation 2.33 would be exact on solution, it is currently unknown how to calculate the exchange function E_{xc} [ρ] exactly. The local density approximation (LDA) is used where, the single particle exchange correlation energy, ϵ_{xc}, is integrated over all space.

$$E_{xc}[\rho] = \int \rho(r)\epsilon_{xc}[\rho(r)]dr \tag{2.33}$$

Several modifications have been made to the LDA to correct non-local effects which are poorly reproduced. One popular combination of corrections is that of Lee, Yang and Parr [31] with the Becke exchange functional, known in the literature as B-LYP (and a later functional became B3-LYP).

2.4.3 Kohn-Sham equations

Obtaining an expression for the kinetic energy of the electrons in terms of the charge density is a harder problem. The first approximation, the local density type of Thomas Fermi approach described above is not sufficiently accurate [32]. It is therefore necessary to break up the charge density into a set of orthonormal orbital functions, as first proposed by Kohn and Sham [33]. These are single particle wavefunctions in a non-interacting system (since interaction terms have been included through Exc). For simplicity here we only consider the spin averaged theory,

$$n(r) = \sum_{\lambda=1,s}^{N} \delta(s_\lambda, s)|\psi_\lambda(r,s)|^2 \int \rho(r)\epsilon_{xc}[\rho(r)]dr \tag{2.34}$$

This means we can now write an expression for T, the kinetic energy, as

$$T = -\frac{1}{2}\sum_{1,s} \int \psi_\lambda^* \bigtriangledown^2 \psi_\lambda dr \tag{2.35}$$

Once the total number of electrons and spin of the system are fixed, these orbitals can be determined using two constraints. Firstly we minimise the energy with respect to the charge density. Secondly different orbitals are kept orthogonal, and normalised through the introduction of a set of Lagrange multipliers, . Therefore we minimise

$$E[n] - \sum_{1,s} E_\lambda \{ \left\{ \int \sum_s \int |\psi_\lambda(r)|^2 dr - 1 \right\} \tag{2.36}$$

Differentiating this with respect to gives

$$-\frac{1}{2}\bigtriangledown^2 \psi_\lambda(r) + \left(v(r) + \int \frac{n(r')}{r-r'}dr' + v_{xc}(r) \right) \psi_\lambda(r) = E_\lambda \psi_\lambda(r) \tag{2.37}$$

where $v(r) = -\frac{1}{2}\sum_{1,s} \frac{Z_\alpha}{|r-R|}$

and $v_{xc}(r) = \frac{\delta E_{xc}[n]}{\delta n(r)}$

It can be seen that equation 2.37 is a single particle Schrödinger equation, as we originally proposed in this section. These three equations together constitute the Kohn-Sham equations, and the self-consistent solution of these leads to the ground state charge density of the system.

Local Density Approximation

The most commonly used and successful approximation is the Local Density Approximation (LDA), first formulated by Kohn and Sham [33] in 1965. If the electron kinetic energy is written as then in the LDA the universal functional is given by

$$F[\rho(\mathbf{r})] = T[\rho(\mathbf{r})] + \frac{1}{2}\int \frac{\rho(\mathbf{r})\rho(r')}{|r-r'|}drdr' + E_{xc}[\rho(r)] \tag{2.38}$$

where $F[\rho(\mathbf{r})]$ universal functional of the electron charge density $\rho(\mathbf{r}), E_{xc}[\rho(r)]$ is the exchange-correlation energy functional and is in equation 2.33.

remember that $E_{xc}[\rho(r)]$ is the exchange and correlation energy per particle of a uniform electron gas of density ρ. The LDA uses the exchange-correlation energy of the homogeneous electron gas, evaluated from the charge density at the point under consideration. Effectively at **r**, $\rho = \rho(r)$ and E_{xc} is equal to the exchange-correlation energy for the electron-gas system which has a homogeneous charge density ρ. This is valid if the inhomogeneity of $\rho(r)$ is small, but the main approximation of LDA is that this is applied even if the inhomogeneity is large. By applying the variational principle to equation $E = \int v(r)\rho(r)dr + F[\rho(r)]$, with the constraint that for an **N** electron system , $\int \rho(r)dr = N$ the following equation is obtained: μ

$$\int \delta\rho(r)\{\frac{\delta T[P]}{\delta\rho(r)} + \nu(\mathbf{r}) + \int \frac{\rho(r')}{|r-r'|}dr' + \frac{\delta E_{xc}}{\delta\rho(r)} - \mu\}dr = 0 \tag{2.39}$$

where $\nu(\mathbf{r})$ is external potential of the ground state of the electron-gas system, and μ is the Lagrangian multiplier equivalent to the chemical potential . Using the

wavefunction $\psi_\lambda(r)$ of the the λ^{th} level, the charge density is defined as :

$$\rho(r) = \sum_{\lambda=1}^{N} |\psi_\lambda(r)|^2 \tag{2.40}$$

which allows the kinetic energy to be defined as:

$$T[\rho(r)] = \frac{1}{2} \sum_{\lambda=1}^{N} \int \psi_\lambda^*(r) \nabla^2 \psi_\lambda(r) dr \tag{2.41}$$

The solution of equation (2.37) is then given by solving the following effective one-electron Schrödinger equation for :

$$\{-\frac{1}{2} \bigtriangledown^2 + v(r) + \int \frac{\rho(r')}{|r - r'|} dr' + \frac{\delta E_{xc}}{\delta \rho(r)}\} \psi_\lambda(r) = \epsilon_\lambda \psi_\lambda(r) \tag{2.42}$$

where ϵ_λ is the energy eigenvalue of the λ^{th} state. This equation is called the Kohn-Sham equation and the eigenvalues are usually identified as the one-electron energy levels (this is an approximation due to LDA's deviation from the real result for states far below the Fermi level [34]. If equation (2.11) is solved self-consistently then the solutions, ψ_λ, will be related to the electron charge density and kinetic energy density via equations (2.8) and (2.9), but the Slater determinant constructed from ψ_λ is not the true many-electron HF wavefunction. ψ_λ are not the same as the one-electron wavefunctions in the Hartree-Fock approximation, but are more directly related to the true electronic charge density.

Generalized Gradient Approximation

Many modern codes using DFT now use more advanced approximations to improve accuracy for certain physical properties. The DFT calculations in this study have been made using the Generalized Gradient Approximation (GGA) [35], [36]. As stated above, the LDA uses the exchange-correlation energy for the uniform electron gas at every point in the system regardless of the homogeneity of the real charge density. For nonuniform charge densities the exchange-correlation energy can deviate significantly from the uniform result. This deviation can be expressed in terms of the gradient and higher spatial derivatives of the total charge density. The GGA uses the gradient of the charge density to correct for this deviation. For systems where the charge density is slowly varying, the GGA has proved to be an improvement over LDA.

2.5 DFT implimentation

Density functional theory is a general approach to the ab initio description of quantum many particle systems, in which the original many body problem is rigorously recast in the form of an auxiliary single particle problem [37]. For the most simple case of stationary problems, DFT is based on the fact that any ground state observable is uniquely determined by the corresponding ground state density ρ, i.e. can be understood as a functional of ρ. This statement applies in particular to the ground state energy, which allows representing the effects of the particle-particle interaction

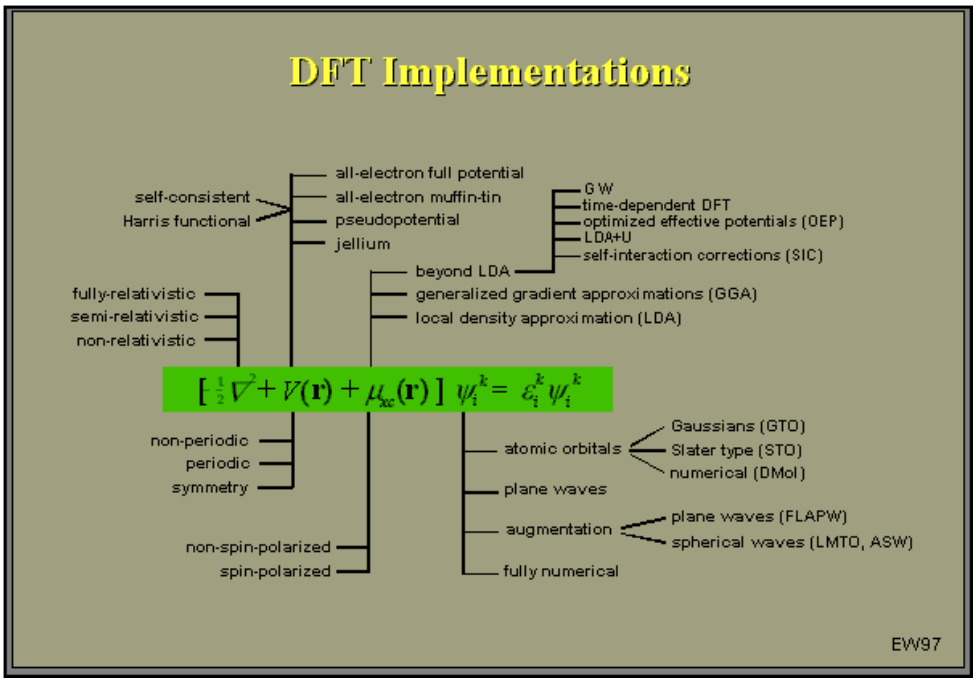

Figure 2.3: The density functional theory implementation[41]

in an indirect form via a density-dependent single-particle potential. In addition to the Hartree (direct) contribution this potential contains an exchange-correlation (xc) component, which is obtained from the so-called xc-energy functional. The exact density functional representation of this crucial quantity of DFT is not known, the derivation of suitable approximations being the major task in DFT.

Extensions of this scheme to relativistic [38] and time-dependent [39] systems, utilizing the four current and the time-dependent density as basic variables, are also available. Furthermore, a DFT approach to quantum hydrodynamics (as a model for the relativistic description of nuclei) has been developed [40].

DFT is an extremely successful approach for the description of ground state properties of metals, semiconductors, and insulators. The success of DFT not only encompasses standard bulk materials but also complex materials such as proteins [42] and carbon nanotubes [43].

The main idea of DFT is to describe an interacting system, its density and not via its many-body wave function. For N electrons in a solid, which obey the Pauli principle and repel each other via the Coulomb potential, this means that the basic variable of the system depends only on three spatial coordinates *x*, *y*, and *z* rather than 3N degrees of freedom.

The major choices for DFT calculations are shown in the Figure 2.3. The center of this figure shows the Kohn-Sham equations, which are the effective one-electron Schrödinger equations of density functional theory. The solutions of these equations give access to the total energy as a functional of nuclear position as well as all properties that can be derived from this theory. The three terms in the square bracket (see Figure 2.3) represent the kinetic energy of electrons, the Coulomb potential due to all charges in the system, and the exchange-correlation potential. The definition of the system and the level of the theoretical approach are given by these three terms. The one-particle wave functions are labeled according to the number of electron level. In a periodic system, the wave functions are characterized by an additional quantum number, **k**, which corresponds to the momentum of the electron in the crystal. The one-electron eigenvalues carry the same labels. DFT calculations for systems with

lighter elements (up to about Z=54) are usually done non-relativistically. It is possible to include relativistic effects through a scalar-relativistic or a fully relativistic description. Scalar relativistic treatment means that the important kinematics effects due to the high kinetic energy of electrons near heavy nuclei are taken into account, but that one averages over the spin-orbit splitting of the electronic levels [45] the Coulomb potential term.

DFT calculations are possible for non-periodic systems. The chemical and structural definition of a system is contained in a collection of atoms such as clusters and molecules and for systems with one, two, and three dimensional periodicity. The use of point or space group symmetry can lead to significant reduction in computational cost as well as to a clear interpretation of the resulting wave functions that reflect this symmetry.

In all electron full potential calculations, the Coulomb singularities arising from the nuclear charges and the full three-dimensional structure of the potential are being taken into account without any approximations. In densely packed systems such as metals and alloys, the effective potential is quite well represented by a muffin tin shaped potential. Around each atom the potential is assumed to be completely spherical up to a certain radius, which is typically about 1 Å. Between these atomic spheres the potential is assumed to be constant. In this approximation, the Coulomb singularities at the atomic positions as well as the steep variation of the potential near the nuclei are still present. Another shape approximation to the potential has become

widely used in the form of pseudopotentials [46]; [47]; [48]; [49]. The objective of pseudopotentials is the elimination of the Coulomb singularities at the nuclear positions and the smoothening of the potential near these singularities. However, no other shape approximations such as constant potentials between the atoms are made in pseudopotential calculations.

2.5.1 Plane-wave (PW) pseudopotential method

The cornerstone of the plane wave pseudopotential method is the expansion of the electronic wavefunctions with the plane wave basis. The computational task is to minimize total energy functional, derived from the DFT, with respect to the coefficients of the plane wave basis set. The success of the PW pseudopotential method originates from iterative diagonalization method [50], [48] which reduce the computational cost of the minimization procedure significantly. For a typical system with 100 basis states and 10000 plane-waves per state this means a reduction of the computational operations by a factor of 100 000, when compared with the conventional direct diagonalization of the Hamiltonian matrix.

It is practical to calculate some of the terms of the total energy functional in real space (r-space) and some of them in the momentum space (k-space). For instance, consider the calculation of the Laplacian in the plane wave basis where the terms involving gradients are easily evaluated in the k-space while in r-space their calculation is not straightforward. The charge density, on the other hand, is easily calculated in

real space, since it is just a square of the magnitude of the wavefunction. The two representations are connected to each other via the Fourier transformation. We have used Fast Fourier Transformation because the transformation between the two spaces is cheap to compute.

The plane wave basis is well suited for the expansion of the smooth valence-electron wavefunctions. In contrast, the core electron wavefunctions (electronic states close to the atomic nucleus) are often sharp and therefore would need a huge amount of plane waves to be expanded properly. However, the effect of the core electrons to the properties of the material does not change significantly as the atom is transferred from one chemical environment to another. Therefore, the obvious solution is to replace the nucleus and the inert core electrons with a pseudopotential which is usually derived from a free atom all electron calculation. The validity of this approximation is well established in a large amount of studies[51].

A further essential part of the PW pseudopotential calculations is the application of supercells, where the system including the defect is enclosed in a so-called supercell satisfying the periodic boundary conditions. If the supercell size is chosen large enough, an approximation of an isolated defect in an infinite lattice is obtained. For further details of the PW pseudopotentials method the reader is asked to see for example the excellent review article by Payne et al. [48].

2.5.2 Bloch's theorem and plane wave basis sets

As yet there has been no mention of how to handle the infinite number of interacting electrons moving in the static field of an infinite number of ions. Essentially, there are two difficulties to overcome: a wavefunction has to be calculated for each of the infinite number of electrons which will extend over the entire space of the solid and the basis set in which the wavefunction will be expressed will be infinite.

The ions in a perfect crystal are arranged in a regular periodic way (at 0**K**). Therefore the external potential felt by the electrons will also be periodic, and it as being same as the length of the unit cell. That is, the external potential on an electron can be expressed as

$$V(r) = V(r+1) \tag{2.43}$$

This is the requirement needed for the use of Bloch's theorem.

Bloch's theorem uses the periodicity of a crystal to reduce the infinite number of one electron wavefunctions to be calculated to simply the number of electrons in the unit cell of the crystal (or half that number if the electronic orbitals are assumed to be doubly occupied, that is spin degenerate). The wavefunction is written as the product of a cell periodic part and a wavelike part

$$\psi_{ki}(r) = \exp(ik.r) f_i(r) \tag{2.44}$$

The first term is the wavelike part which will be discussed below. The second term is the cell periodic part of the wavefunction. This can be expressed by expanding it into a finite number of plane waves whose wave vectors are reciprocal lattice

vectors of the crystal

$$f_i(r) = \sum_G C_{\mathbf{i}} G \exp(iG.r) \tag{2.45}$$

where are the reciprocal lattice vectors which are defined by for all where is a lattice vector of the crystal. Therefore each electronic wavefunction is written as a sum of plane waves

$$\psi i(r) = \sum_G C_{\mathbf{i}}^{k+G} \exp[i(k+G).r] \tag{2.46}$$

By the use of Bloch's theorem, the problem of the infinite number of electrons has now been mapped onto the problem of expressing the wavefunction in terms of an infinite number of reciprocal space vectors within the first Brillouin zone of the periodic cell, . This problem is dealt with by sampling the Brillouin zone at special sets of **k**-points

The electronic wavefunctions at each **k**-point are now expressed in terms of a discrete plane wave basis set. In principle this Fourier series is infinite. However, the coefficients for the plane waves, Ci, $^{K+G}$, each have a kinetic energy (*K*e)

$$Ke = \frac{\hbar^2}{\mathbf{2m}} |\mathbf{K} + \mathbf{G}|^2 \tag{2.47}$$

The plane waves with a smaller kinetic energy typically have a more important role than those with a very high kinetic energy. The introduction of a plane wave energy cutoff reduces the basis set to a finite size.

This kinetic energy cutoff will lead to an error in the total energy of the system but in principle it is possible to make this error arbitrarily small by increasing the size

of the basis set by allowing a larger energy cutoff. The cutoff that is used in practice depends on the system under investigation.

Another advantage of expanding the electronic wavefunctions in terms of a basis set of plane waves is that the Kohn-Sham equations take a particularly simple form. Substitution of equation (3.24) in to the Kohn-Sham equations, (3.17), gives

$$KS = \sum_{G'} \{ \frac{\hbar 2}{\mathbf{2m}} |\mathbf{K} + \mathbf{G}| \, \delta'_{\mathbf{GG}} + V_{\mathbf{ion}}(G - G')$$

$$+ V_{elec}(G - G') + V_{ex}(G - G') \} X \, \mathrm{Ci}, K + G' = \boldsymbol{\varsigma \mathbf{i}} \, \mathrm{Ci}, ^{\mathbf{K}+\mathbf{G}'} \tag{2.48}$$

It can be seen in this form that the reciprocal space representation of the kinetic energy is diagonal and the various potentials can be described in terms of their Fourier components. Usual methods of solving the plane wave expansion of the Kohn-Sham equations is by diagonalisation of the Hamiltonian matrix whose elements are given by the term in curly brackets. It follows that the size of the Hamiltonian matrix is determined by the energy cutoff (K_c)

We would show that it is not necessary to solve this by conventional matrix diagonalisation techniques, but a more computationally efficient method exists where the plane wave coefficients are treated as dynamical variables.

2.6 CASTEP

CASTEP (Cambridge Serial Total Energy Package) is a software package [52] which uses density functional theory (DFT) to provide a good atomic-level description of all manner of materials and molecules. CASTEP can give information about total energies, forces and stresses on an atomic system, as well as calculating optimum geometries, band structures, optical spectra and much more. It can also perform molecular dynamics simulations.

CASTEP is an ab initio (first principle) quantum mechanical program employing DFT to simulate the properties of solids, interfaces, and surfaces for a wide range of materials classes including ceramics, semiconductors, and metals. First principle calculations allow researchers to investigate the nature and origin of the electronic, optical, and structural properties of a system without the need for any experimental input other than the atomic number of mass of the constituent atoms. CASTEP is a computational programme package well suited to research problems in solid-state physics, materials science, chemistry, and chemical engineering where researchers can employ computer simulations to perform virtual experiments, which can lead to tremendous savings in costly experiments and shorter developmental cycles.

2.7 GULP

GULP(General Utility Lattice Program) [53] is a program for performing a variety of types of simulation on 3D periodic solids, gas phase clusters and isolated defects

in a bulk material. In particular it is designed to handle both molecular solids and ionic materials through the use of the shell model. One difference between GULP and other similar programs is that symmetry is used for solids to accelerate the calculations and to simplify the input. This can lead to up to an order of magnitude improvement in computational efficiency. This features subsequently allows for a simultaneous multi structural fit routine.

2.7.1 MARVIN

MARVIN (Minimization And Relaxation of Vacancies and Interfaces for Neutral Surfaces) program was developed at Royal Institution of Great Britain for studying surfaces and interfaces. MARVIN is based upon a similar code MIDAS developed by Taser in the late 1970's. It has capability of calculating the surfaces energies and also allows the introduction of ions and molecules to the surfaces, which is important in modeling crystal growth and catalysis. This code considers a simulation cell of a finite number of atoms, which are repeated in two dimensions. The cell consist of a region I and II. In this regard Marvin relax region I atoms explicitly whereas those in Region II remain fixed. The total energy of the system defined as the energy of all the regions I structural units, all the regions II structural units and periodic image of both.

Chapter 3
Prediction of crystal structures

In this chapter we will focus on the prediction of structural parameters, e.g.

testing the potentials of CaS in atomistic simulation since they were never used before, sampling the K-point mesh, determining cutoff energy in DFT calculation, determining the radii size using Mott-Littleton technique involving atomistic calculations, determining the surface stability of different surfaces in both DFT and atomistic calculations.

3.1 Bulk structure and properties

CaS and CaO have cubic rock salt structure as shown in figures 3.1 and 3.2 respectively, with eight atoms per unit cell. The lattice parameters of CaO and CaS are predicted and compared with experiments and previous calculations. As shown in Figure 3.1, Oxygen (red colour) and Calcium (blue colour) are the building blocks of CaO, and for CaS there is Calcium and Sulphur (yellow). These compounds are insulators, and that means they have a sufficiently large bandgap as compared to other semiconductors and metals. The densities of CaO and CaS are 3340 kg/m^3 and 2600 kg/m^3 respectively, and the melting point of CaO is 2900^{0}C, and that for CaS is 2400^{0}C. The high melting points of these compounds show clearly that they have high heat resistivity and consequently they can be applied at a very high tempera-

ture in industrial applications. The structural optimization of CaO and CaS systems has been performed in both ab initio (DFT) and atomistic simulations. Lattice parameters have been varied and the most stable value has been calculated to be 4.805Å and 5.747Å for CaO and CaS respectively as shown in Figure 3.3. Both values of CaO and CaS lattice parameters compare well with experimental values 4.810Å **[55]**, 4.165Å **[56]** for CaO and 5.690Å for CaS **[55]**. These values have been obtained by using atomistic simulation method. For DFT calculations where done on default and GGA functional has been applied in all calculations. Structural optimizations were performed at absolute zero temperature (0K) for DFT and atomistic simulation calculations. Using the same lattice constant we have managed to calculate bulk modulus. The bulk modulus is given by the ratio of pressure to the relative decrease in volume. The bulk moduli of CaO and CaS obtained using atomistic simulation at equilibrium values are 81.2 GPa and 56.0 GPa respectively. These values are compared with the results obtained using DFT calculations at 100 GPa and 128 GPa for both CaO and CaS bulk modulus, where 56.12 GPa [56] and 62.12 GPa [58] were obtained respectively.

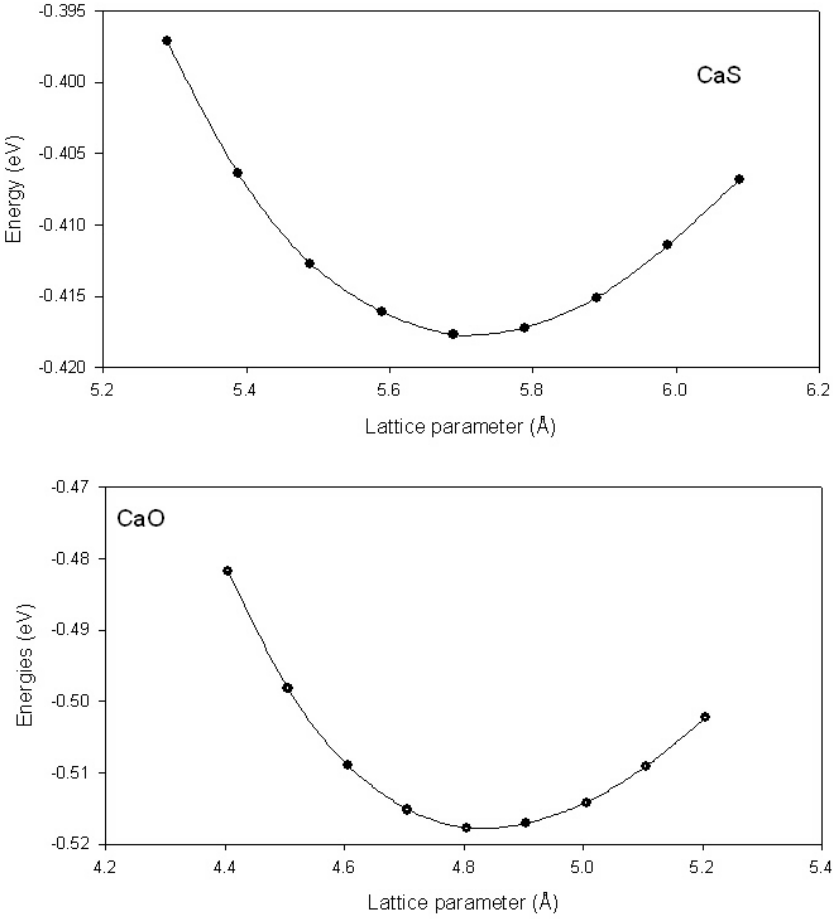

Figure 3.1: The graphs of energy vs lattice parameter of CaO and CaS (Atomistic simulation method).

Table A - Short-range potentials

Interaction of ions	A(eV)	r(Å)	C(eVÅ6)	Potential cutoff (Å)
O shel O	22764.0000	0.149000	27.8800	12.000
O shel Ca	1228.9000	0.3372	0.0000	12.000
Ca charges = 2.0000				
S core = 0.848190				
S at shell = -2.848190				
Spring constant = 74.720380				

Table B

Ca core S	704.71153	0.430154	0.0000	12.000
O shel S	9398.0000	0.149.0000	120.80827	12.000
Ca charges = 2.0000				
S core = 0.568500				
S at shell = -2.568500				
Spring constant = 13.838260				

Table 3.1: The Potential parameter derived by Lewis and Catlow in table A and K Wright in table B (Unpublished.)

3.2 Atomistic calculations

3.2.1 Potential parameter used in this study

The atomistic simulations for this study used Buckingham potentials type that was fitted to experimental values. These potentials were used in various structural calculations, and have proven to be valid since they reproduce experimental values and those from other computational methods as well. Potential parameters used in this study have been derived by Catlow and Lewis (CaO) [69] and Wright (CaS) unpublished. Since CaS potentials were never used before, they will be tested in this study for validity of yielding the necessary thermodynamic properties. Study for validity of yielding the necessary thermodynamic properties.

3.2.2 K-points sampling

In the atomistic method we sampled 4x4x4, 6x6x6, 8x8x8 and 10x10x10 k-points. We have chosen 10x10x10 k-points since it is more accurate and can be handled by the supercomputer. These k-point values will be applied in all atomistic calculations to investigate other structural properties. This k-point sampling will help in simulating the material so that it gives results that are comparable with other experimental and computational methods.

3.2.3 Radii variation in atomistic simulation

The region size sampling method in the Mott-Littleton approach helps to control the interaction around the defect centre (region one) without introducing major effect on region two. When the defect is introduced in the crystal structure, it causes disruption of the system. By varying the region one size, we attempt to ensure that the disruption caused by introduction of the defect occurs in this region (region one) only. We further carried out a convergence test to ascertain that defect energies will not change by more than a small amount as shown in Figure 3.4, that the size of region one is increased. The calculated results in Figure 3.4 show that the region 1 size that gives the lowest energies is 9Å. The values obtained were applied in all systems to investigate other structural properties in this study.

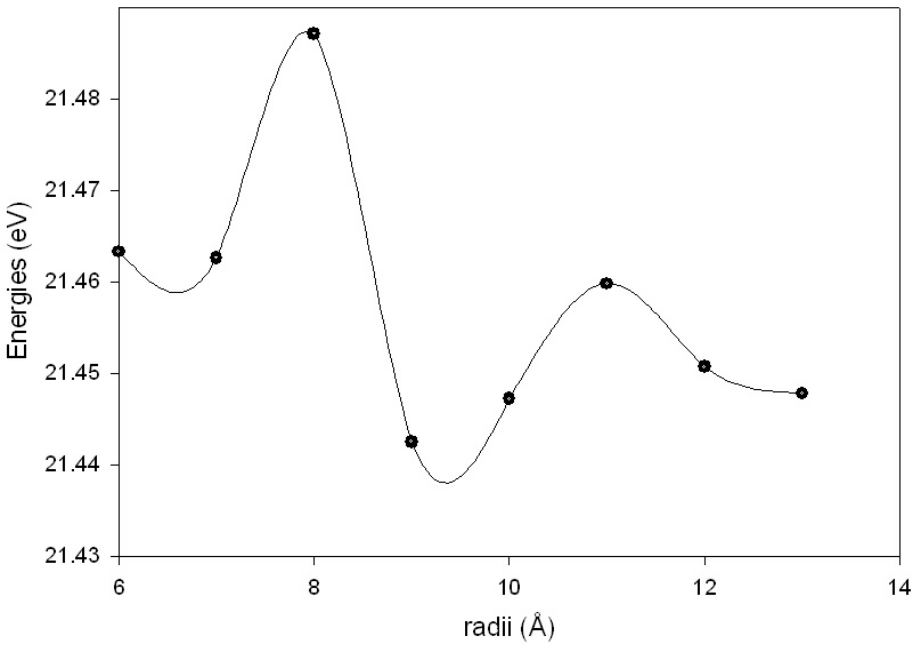

Figure 3.2: Energy (eV) vs region size variation (Å)

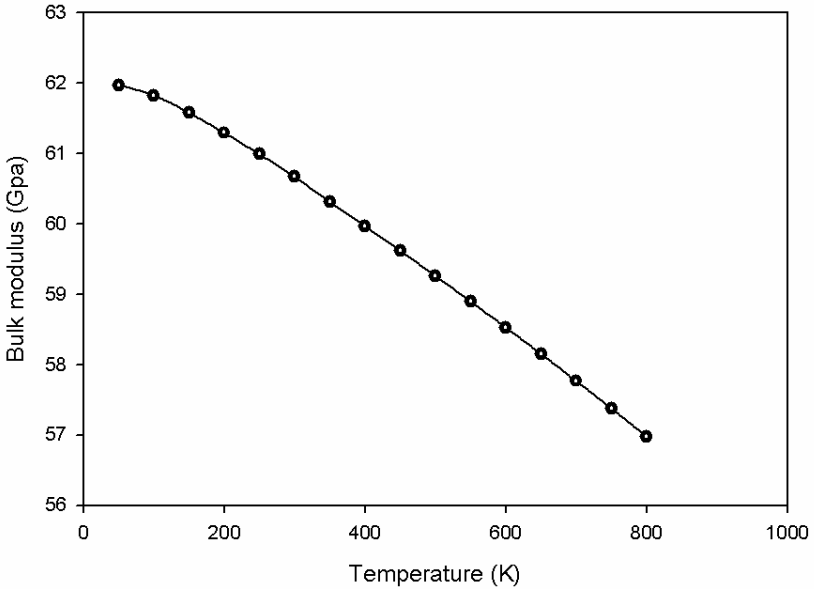

Figure 3.3: Bulk modulus vs temperature in CaS systems

3.2.4 Dependence of potential parameters on the crystal structures of CaS

CaS potentials derived by Wright (unpublished) have been tested in this study since they were never used before. The potentials were fitted using the atomistic simulation methods and the calculations were performed to yield various thermodynamic parameters, e.g. temperature, bulk modulus and volume etc.. Generally, the calculated values agree reasonably with the experimental thermodynamic quantities. The equilibrium lattice parameter of CaS obtained from this calculation is 5.667Å (figure 3.2), and it compares well with 5.689Å from the experiment [66].The calculated lattice parameter, from this study, using DFT is 5.747Å. The bulk modulus of CaS

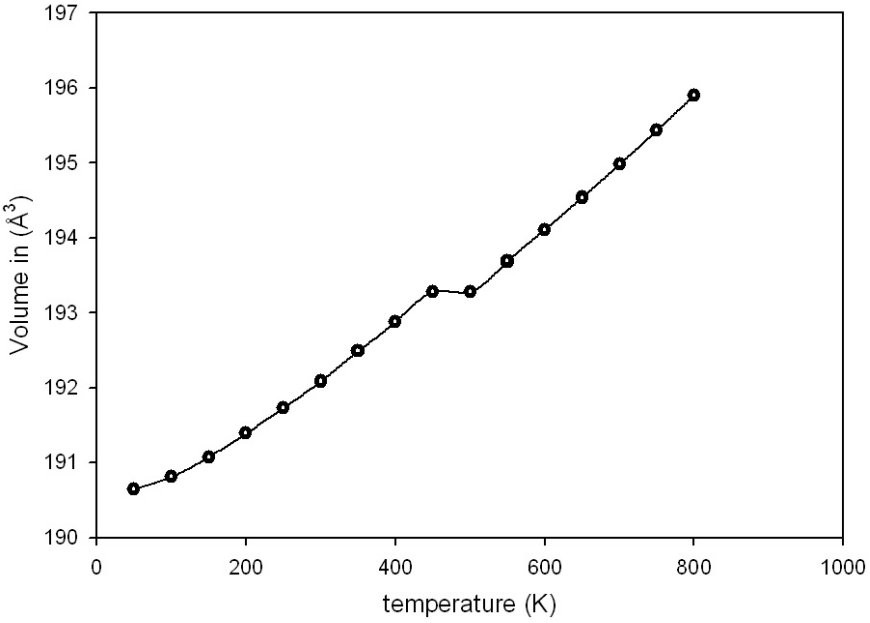

Figure 3.4: Volume of a unit cell vs temperature in CaS system

obtained using the atomistic method is 62.12 GPa and this value compares well with 64.00 GPa from experiment by [66]. All graphs shown in this study depict similar trends as those predicted by Cortona et al [67]. Figure 3.5 shows the variation of the bulk modulus of CaS with temperature, and as expected it becomes softer as the temperature increases. The bulk modulus of CaO obtained from this study is 137.1 GPa. This compares reasonably well with 109.0 GPa from DFT calculations [69]. The calculated lattice parameter of CaO is 4.805 Å and this also compares well with 4.810Å [55] and 4.8163Å [68] from experiment. Figure 3.6 shows the relationship between volume and temperature at zero pressure, and all predictions were carried out using the potentials derived by Lewis and Catlow [69] listed in table 3.1. We have, generally, confirmed the reliability of the CaS and CaO potentials by reproducing certain experimental thermodynamic properties. We are consequently confident to extend atomistic simulation studies to other structural properties using these potentials.

3.3 CASTEP calculations

3.3.1 K-points sampling

Calculations can be done at a finite number of k-points shown in Figure 3.7. Owing to time limitations, it is necessary for the structure to converge within a reasonable time, and consequently a reasonable number of k-points values are needed. An increase in k-points on the system, results in the system requiring more memory. Due

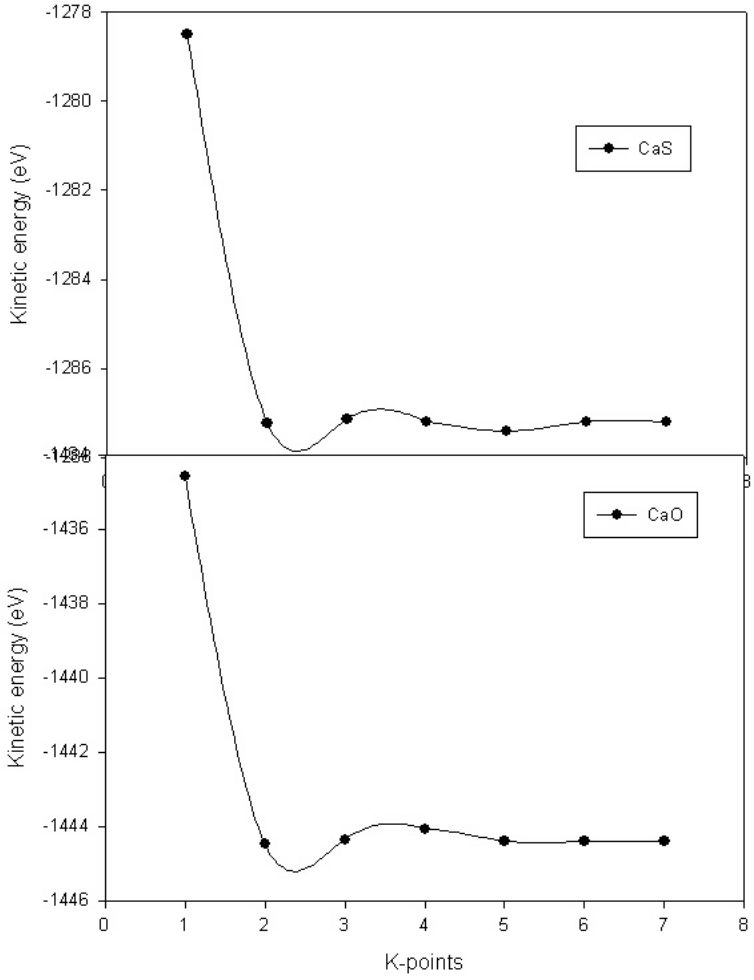

Figure 3.5: Kinetic energy vs K-Points sampling of CaS and CaO systems

to the memory limitation, we have tried to determine the lowest values of k-points that can perform accurate calculations in a supercomputer. The results obtained show clearly how we sample the k-point mesh in the system. Ultrasoft pseudopotential, in DFT, would determine the accuracy of k-points sampling. For calculations in the current study, we have used Monkhorst and Pack (1976 k-points sampling [70]. In DFT calculation, k-points were determined using chosen energy cutoff (250 eV). Several calculations were done using single point energy minimization to sample k-points values that give good structural prediction of the results and that will compare well with the experiment. In DFT, we have obtained 3X3X3 k-points values as shown in Figure 3.7 for both CaO and CaS systems. The same parameters were used to predict other structural properties. In surface application we have used 3X3X1 k-points sampling to reproduce similar results because we found that the lattice parameter of a = b, however, c is much larger than in the bulk.

3.3.2 Cutoff energy for convergent calculations

Using the k-points sampling determined from the previous subsection 3.2.2, the cutoff energy was determined by performing a series of calculations as shown in Figure 3.8. From this minimum energy cutoff, we have investigated other structural properties that would give us the most comparable results with experiment. As shown in the Figure 3.8, it can be deduced that the convergence is achieved as from 350eV; hence we will consider 450eV as our cutoff energy in this study. The energy cutoff deter-

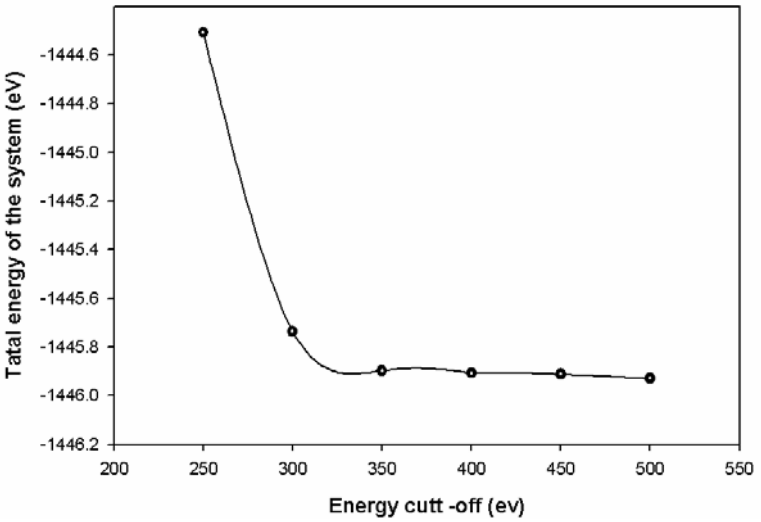

Figure 3.6: Total energy of CaO vs energy cut-off

mined, as indicated in the graph will be used to predict other structural properties in this study.

3.4 Comparing the two methods

3.4 In the Table 3.2, we compare the DFT and atomistic calculations. The results obtained show the correlation of these two methods. Lattice parameters for both

Crystal structure	*Lattice parameter* (Å)		*Bulk Modulus (GPa)*		*Lattice*.parameter *Exp.* (Å)	
	DFT	Atomistic	DFT	Atomistic	Ref[55]	Ref[56]
CaO	4.805	4.805	100	128	4.810	4.165
CaS	5.747	5.667	56	62	5.690	

Table 3.2: The Table comparing results for DFT and atomistic calculations

methods are comparable with other cited results for both CaS and CaO [55], and CaO [56]. These results give us confidence in investigating other structural properties using this method.

3.5 Surface calculations

3.5.1 Convergent test for the (100) surfaces layers

In our previous atomistic study the planewave pseudopotential calculations for both

bulk CaS and CaO showed good agreement of the lattice parameters with other calculations [68]. The planewave pseudopotential method was further used to determine the number of layers to be considered in surface energy studies. Geometry optimization was performed for several numbers of layers and corresponding surface energies were calculated. The CaO (100) surface, as shown in Figure 3.9 indicates that we can consider at least three layers. Since on this study we want the orientation of oxygen atom on the top layer to be at the centre of Ca's, then we will add extra layer that will make three and half layers (seven layers). The adsorption of molecules would be done on three and half layers of both CaO (100) and CaS (100) surfaces, where each layer consists of two atoms. The stability of these surfaces agrees well with similar work done by de Leeuw et al [4] using a different computational method (Metadise code).

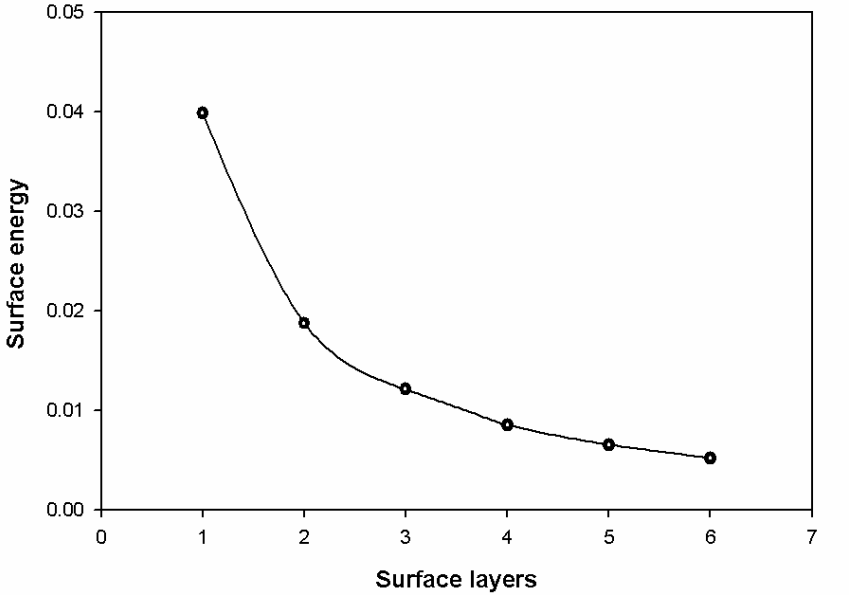

Figure 3.7: The convergence of the surface energy with the number of layers of CaO (100)

Surfaces	DFT Calculation (KJ/mol	Atomistic Calculations KJ/mol	METADISE(KJ/mol)[4]
CaO (100)	0.949	0.750	0.770
CaO (110)	1.188	1.970	1.950
CaO (111)	3.945	4.830	2.470
CaO (140)	0.983	1.035	
CaO (130)	1.016	1.148	1.150
CaS (100)	0.796	0.437	
CaS (110)	1.012	1.109	
CaS (111)	1.897	1.536	

Table 3.3: Table that indicates the stability of different surfaces of both CaO and CaS.

3.5.2 Stability of surfaces layers for DFT and atomistic calculations

The surface energies of the low index surfaces (100), (110) in (111) and table 3.3 suggests that the (100) surface layer is the most stable surface and (111) is the least stable surface for both CaO and CaS using both methods of calculation. This prediction is in agreement with other previous interatomic potentials calculations [4]. This agreement also gives us confidence in working with surfaces to investigate other surface properties. We shall use DFT method to study the (100) surface for adsorption of molecules and atomistic calculation shall be employed to investigate all surfaces.

3.6 Summary

The prediction of structural properties using both DFT and semi atomistic methods show that the most stable surfaces are CaO (100) and CaS (100). We have therefore decided, from these results, to consider investigation of the adsorption behaviour of molecules at different coverage's on such surfaces. In the testing of Wright's poten-

tials, employed in this study, expected thermodynamic parameters (e.g. temperature, volume and bulk modulus) have been well reproduced. According to the results, we have to consider CaO (100) and CaS (100) to investigate the adsorption behaviour of molecules in DFT calculations.

Chapter 4
Atomistic simulation calculations of CaO and CaS

4.1 Introduction

Atomistic simulations are well suited for calculations of the structure and relative stability of a whole range of metal oxides. However, the high temperatures and pressures found within the earth make the use of simulation even more appealing because experiments are often difficult and subject to a high degree of error. It is always ensured that CaO and CaS systems are handled with care so that they can represent real existing system. In this case we even calculated the radius variation of both region one and region two on the bulk crystals of both CaS and CaO structures. The detailed information of this approach will be given and defect energies will be calculated by applying Mott-Littleton method in GULP code. Migration of atoms from lattice position to vacant position will be explained in this chapter. The activation energy will be determined from graphs shown in this chapter. Surface energy is the energy required to cleave the surfaces of a bulk system. As explained in the previous chapter, different surfaces layers will be considered. The number of surface layers required to achieve convergence will also be considered. The introduction of foreign atoms on the surface and their impact will be discussed in this chapter.

4.2 Introduction of defects and diffusion

Table 4.1 and Figures 4.1- 4.4 show the migration path of atoms within the crystal structures of CaS and CaO systems. This migration path has been obtained by moving an atom from lattice site via interstitial site to an adjacent lattice vacancy. This describes the simplest path preferred by an atom when migrating from one vacant position to the other with a minimum interacting energy with the surrounding atoms. The activation energy is defined as the energy required for overcoming the barrier for the diffusion process to occur as shown in Figures 4.1- 4.4. On the graph we have determined the activation energy as the difference in minimum and maximum energies on the plotted graphs, where we have the energy at the saddle point, and the energy

at initial configuration, with one site vacant. In Figure 4.4, we note the difference from other related plots, (Figures 4.1-4.3), and this, we attribute to the fact that oxygen atom does not migrate smoothly in CaO as other atoms do (i.e. S in CaO, S in CaS and O in CaS bulk crystals). The trend of activation energies of O and S in both CaO and CaS crystals obtained in this study does not have direct comparison with either experiment or

other computational calculations. The only comparison can be with diffusion of other molecules in the same systems. Activation energies of O in CaO, S in CaO, O in CaS and S in CaS are 176.737kJ/mol, 116.049kJ/mol, 86.340kJ/mol and 124.930kJ/mol respectively. The activation energy from experiments, was obtained when the migration of H_2S and SO_2 molecules occurred in the bulk crystal

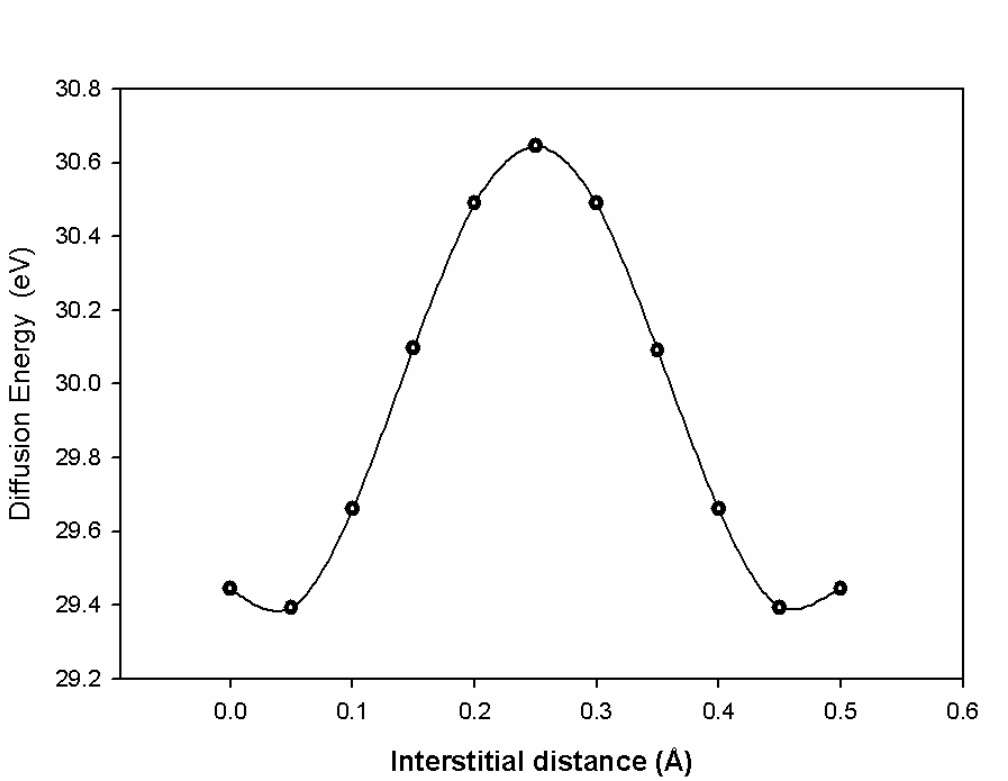

Figure 4.1: The diffusion of S in CaO bulk crystal

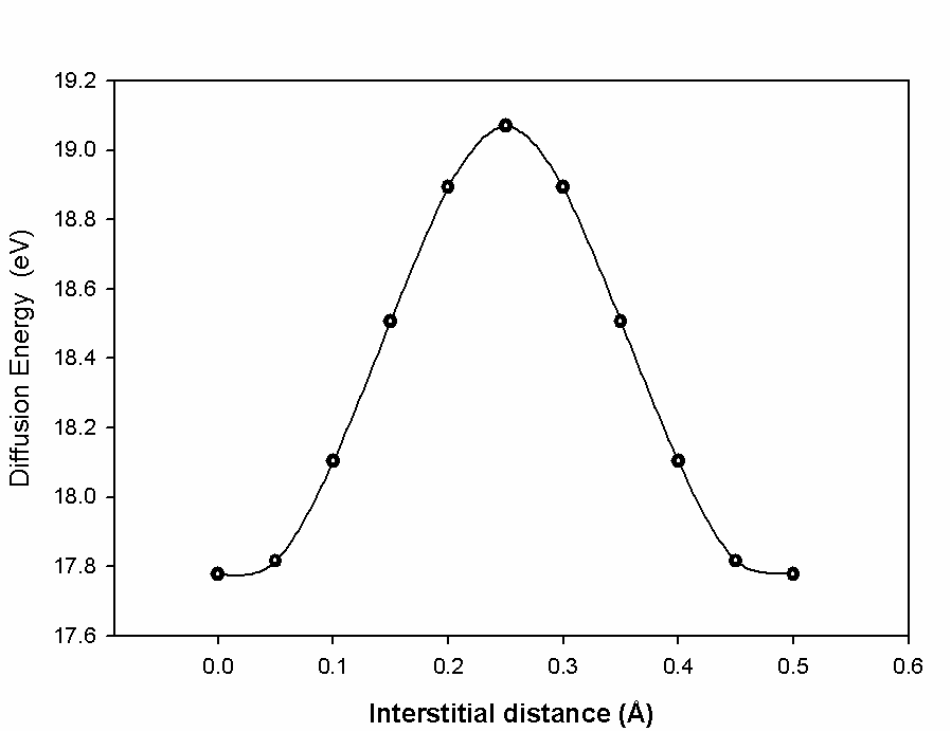

Figure 4.2: The diffusion of S in CaS bulk crystal

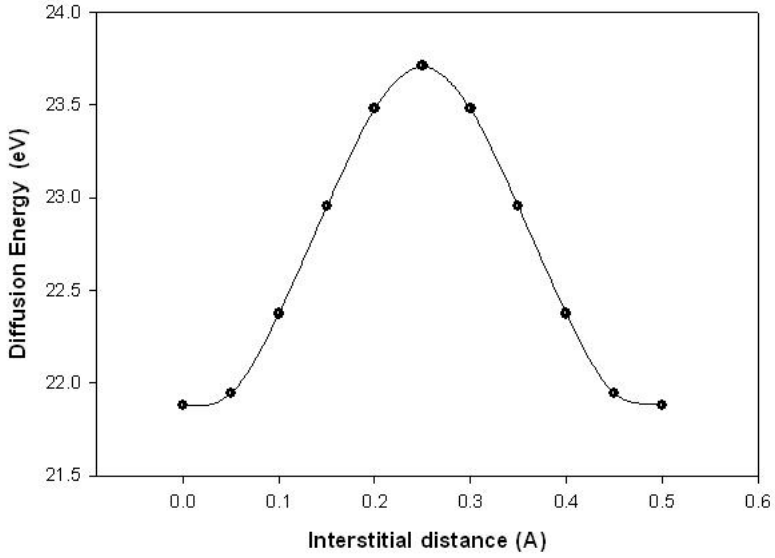

Figure 4.3: The diffusion of O in CaS bulk crystal

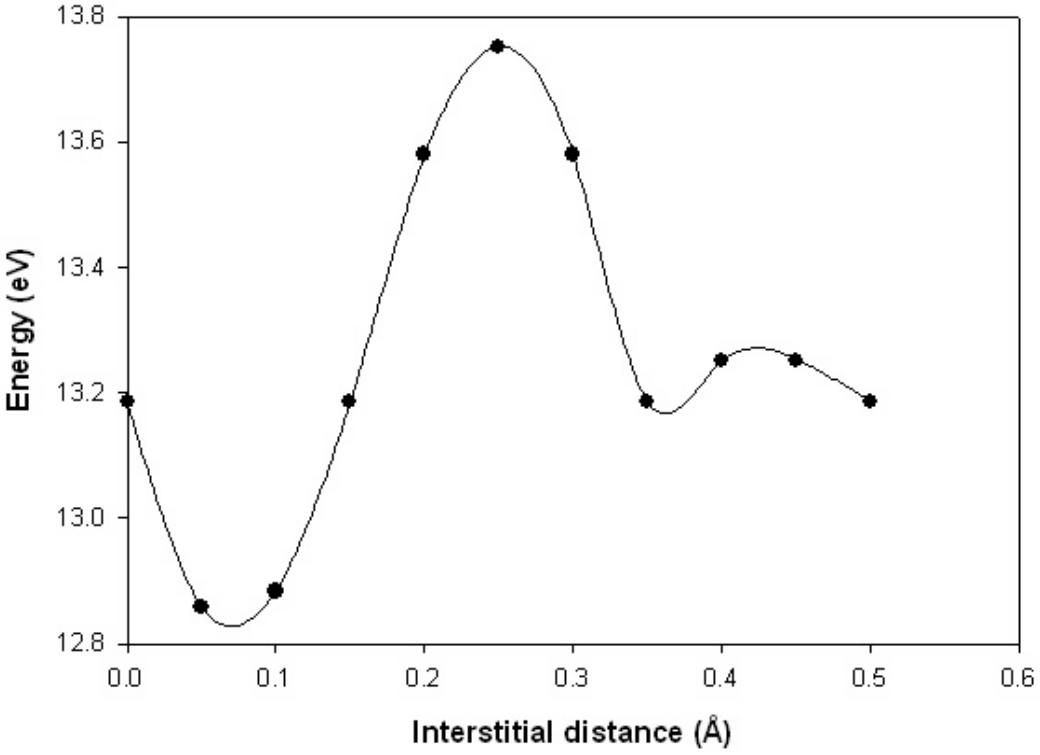

Figure 4.4: The diffusion of O in CaO bulk crystal

Defects	Type	CaO (eV)	CaS (eV)
Ca	Interstitial	-9.88	-8.88
	Vacancy	21.45	17.19
	Schottky	-22.70	-24.10
	Frenkel	11.57	8.31
	Interstitial	-10.39	
O	Vacancy	21.84	
	Impurity		-5.19
	Frenkel	11.45	
	Interstitial		-9.62
S	Vacancy		17.03
	Impurity	7.86	
	Frenkel		7.45

Table 4.1: Calculation of defects energies using atomistic technique.

of calcined limestone, ranging between 25 (104.67) to 43 kcal/mol (180 kJ/mol). Borgwardt et al [2] obtained the activation energy of 42 kcal/mol in the study of the reaction of H_2S and sulphur with the limestone. The results were obtained at the temperature of 750^0 C, with the particle size in the range 1.6-1.00μm. Even though the comparison does not pertain to the same crystal, it gives a good idea since they belongs to the same category of oxides.

4.3 Defects formation in CaO and CaS crystals

A defect is created during the removal or addition of an extra atom in the crystal and the total energy of the system are altered. After the addition of defects, the system experiences structural relaxation. The defect formation (Vacancy, Interstitial and impurity) are calculated according to equation 4.1 on the relaxed bulk systems given by:

$$E_{defects} = E_{with-defects} - E_{without-defects} \tag{4.1}$$

where $E_{defects}$ it the total defect energy of the relaxed system, $E_{with-defectsDEp}$ is the total energy of the relaxed system without defect and $E_{withiout-defects}$ is the total energy of the relaxed system with defect.

The formulae defined in equation 4.1 were used to calculate defect (Vacancies, interstitilas and impurities) energies shown in CaO and CaS are shown in the table 4.1, and for Schottky and Frenkel Defects were calculated by equation 4.2 and 4.3 respectively. The equations are given by:

$$Schottky\_Def = E(total\_energy\_of\_Vac) + E(Latt\_Energy) \tag{4.2}$$

$$Frenkel\_Def = E(Vac) + E(Inter) \tag{4.3}$$

The results in table 4.1 reflect the energies required to form a defined defect in CaO and CaS.

The formation of vacancies in the CaO and CaS bulk crystal as shown in table 4.1 is energetically less demanding compared to the addition of atoms at the interstitial site in the same bulk crystals of CaO and CaS. Addition of foreign atoms in the crystals constituted impurities, e.g. addition of oxygen atom in CaS bulk crystal and sulphur atom in the CaO bulk crystal. The formation of an impurity in the mentioned bulk crystal is less demanding compared to the formation of defects on the interstitial site. We have also calculated the Schottky and Frenkel using equations 4.2 and 4.3

Surface energy of CaS (100) and CaS (100) with defect(s) on the surface layer			
Quantity of Defects	CaO (100) kJ/mol)	Quantity of Defects	CaS (100) kJ/mol)
0 S	0.823	0 Ox	0.437
1 S	-12.891	1 Ox	-0.110
2 S	-29.428	2 Ox	-0.726
3 S	-39.819	3 Ox	-1.173
4 S	-43.112	4 Ox	-1.924
5 S	-50.612	5 Ox	-2.959
6 S	-63.172	6 Ox	-3.307
7 S	-89.554	7 Ox	-3.923
8 S	-105.91	8 Ox	-9.344

Table 4.2: The surface energies of CaO (100) and CaS (100) and how they are affected by an increase in coverages of both Oxygen and Sulphur on the surfaces.

respectively to justify our discussion of defects. As shown on Table 4.1, the results suggests same predictions given by the vacancies and intestinals results as discussed above.

4.4 Doped surfaces of CaS (100) and CaO (100)

Doped surface layers of CaS (100) show similar trends when compared to the doped surface layers of CaO (100) in Table 4.2. The surface energies of both surfaces decrease with an increase in the percentage coverage on the surface layers. It is apparent that the CaO (100) surface energies became negative as the coverage of S increases. Similarly, CaS (100) surface energies follow the same trend as the oxygen coverage increases. According to de Leeuw et al [4], when the surface energy changes to negative values, as shown in Table 4.2, the bulk crystal becomes unstable. The negative stability suggests that the surface collapses as the coverage of atoms increases on the surface. Consequently, the formations of both CaO and CaS on the surfaces

Surface energy of CaS with defect(s) at edge position(s)		
Quantity of defects on the layer	CaS (110) kJ/mol	CaS (510) kJ/mol
1 Ox	0.636	0.419
2 Ox	0.172	0.297
3 Ox	-0.376	0.179
4 Ox	-0.847	0.058
5 Ox	-1.233	-0.061
6 Ox	-1.817	-0.181
7 Ox	-2.147	
8 Ox	-2.917	

Table 4.3: The surface energies of CaS and how they one affected by an increase in coverage of Oxgen on the edge position.

were formed spontaneously. The atom-atom exchange of O with S is more exothermically favourable since the surface energy becomes more negative as the coverage increases on both CaO (100) and CaS (100) surface layers. From the results obtained in this work, we deduce that the surface became more stable than the bulk, and as a result it predicts the spontaneous formation of CaS on the surface. Similarly spontaneous formation of CaO occurs on the surface of CaS (100), since they follow a similar trend of negative surface energies. This implies that the atom-atom exchange of O and S is more exothermically favourable.

4.5 Doped surfaces of CaO (110) and CaS (110) on both edge and valley

The surface energies of CaO (110) on the edge position in Table 4.4 give opposite trends as compared to CaS (110) on the edge position in Table 4.3. The oxygen percentage coverage on surface layers of CaS is favourable up to 25%, as from 37.5%

Quantity of defects	Surface energy of CaO with defect(s) at the edge position(s)	
	CaO (110) KJ/mol	CaO (510) KJ/mol
1 S	2.674	1.212
2 S	3.426	1.420
3 S	4.059	1.592
4 S	4.837	1.801
5 S	5.559	1.975
6 S	6.443	2.184
7 S	7.183	2.358
8 S	8.082	2.568

Table 4.4: The surface energies of CaO and how they are affected by an increase in sulphur coverage on the edge position.

Surface energy of CaS with defects at the valley positions		
Quantity defects on the layer	CaS (110) KJ/mol	CaS (510)KJ/mol
1 Ox	0.645	0.419
2 Ox	0.114	0.317
3 Ox	-0.376	0.179
4 Ox	-0.727	0.099
5 Ox		-0.077
6 Ox	-1.514	
7 Ox		
8 Ox	-2.547	

Table 4.5: The surface energies of CaS and how they are affected by an increase in Ox coverage on the valley position.

Surface energy of CaO with defects at the valley positions		
Quantity defects on the layer	CaO (110) kJ/mol	CaO (510)kJ/mol
1 S	0.855	1.280
2 S	1.145	1.420
3 S	1.443	1.759
4 S	1.342	1.998
5 S	1.542	2.246
6 S	2.301	2.494
7 S	2.583	2.743
8 S	2.874	2.992

Table 4.6: The surface energies of CaO and how they are affected by an increase in S coverage on the valley position.

Surface energy of CaS (111) for the terminated surfaces		
Qunatity of defects on the layer	CaS (111)^{Ca} kJ/mol	CaS (111)^{S} kJ/mol
0 Ox	1.412	1.375
1 Ox	0.032	0.912
2 Ox	0.477	0.470
3 Ox	0.032	0.019
4 Ox	-0.399	-0.412
5 Ox	-0.820	-0.812
6 Ox	-1.245	-1.175
7 Ox	-1.633	-1.562
8 Ox	-2.025	-1.913

Table 4.7: The surface energies of CaS (111) and how they are affected by an increase in coverage of both Calcium, Sulphur with Ca for Calcium terminated surface and S for Sulphur terminated surface

the formation of CaO starts to be favourable like the formation of CaS on the CaO (100) surfaces layers. On CaS (110) surface layers, the coverage became more stable on the valley than on the edge. This implies that the formation of CaO is favoured on the valley than on the edge. On doping at both edge and valley positions (Table 4.4 and 4.6), theCaO (110) becomes unstable as the sulphur coverage increases, while the stability increases on the CaS (110) with the increase in the oxygen coverage up to certain percentages. An increase in the instability of the CaO (110) surface decreases the formation of CaS on the surfaces. From this we deduce that the formation of CaS on the CaO (110) is not favoured.

4.6 Doped surface of CaO (111) and CaS (111)

The instability of CaO (111) surfaces as shown in Table 4.8 increases as the percentage of S coverage increases. This implies that the formation of CaS on CaO (111)

Qunatity of defects on the layer	Surface energy of CaO (111) for the terminated surfaces	
	CaO (111)^{Ca} KJ/mol	CaO (111)^{Ox} KJ/mol
0S	2.778	2.741
1S	3.026	3.391
2S	3.723	4.044
3S	4.057	4.210
4S	4.864	5.129
5S	5.273	5.166
6S	6.107	5.578
7S	6.651	6.540
8S	7.801	8.588

Table 4.8: The surface energies of CaO (111) how they are affected by an increase in coverage on both Calcium, Oxygen with Ca for Calcium terminated surface and Ox for Oxygen terminated surface

surface is not favoured. Table 4.7 depicts how the stability of CaS (111) increases as the percentage coverage of O increases. This shows that the CaO is likely to be formed on the S-vacancy of CaS (111). In comparison, the formation of CaS on CaO (111) surfaces is preferable on the Ca-terminated surface than on the O-terminated surface up to 50% coverage. Above such percentage coverage, the formation of CaS appears to be favourable on the O terminated surface. However, the percentage coverage of O on the CaS increases up to 50%, after which the surface collapses. This implies that the formation of CaO on the CaS (111) surface layers is favoured in the bulk crystal than on surfaces. On the CaO (111), the stability is not favoured for both Ca-terminated and O-terminated surfaces at all indicated S coverage's. This implies that the formation of CaS on the CaO (111) surfaces is not favoured on the two terminations.

4.7 Doped surface CaO (510) and CaS (510)

Figures 4.5 and 4.6 show the structures of CaO (510) with the sulphur (S) located at the valley and edge positions respectively. The same figures will be used to explain the CaS (510) surface since the crystal structures are similar. In the same way as CaO (110) and CaS (110) surface layers, the stability of the CaO (510) surface (Table 4.4) decreases as the S coverage on the edge increases. Similarly the stability of CaS (510) (Table 4.6) reduces at the S coverage in the valley increases. However in table 4.5 the stability of CaS (510) surface is enhanced with the increase of oxygen coverage,

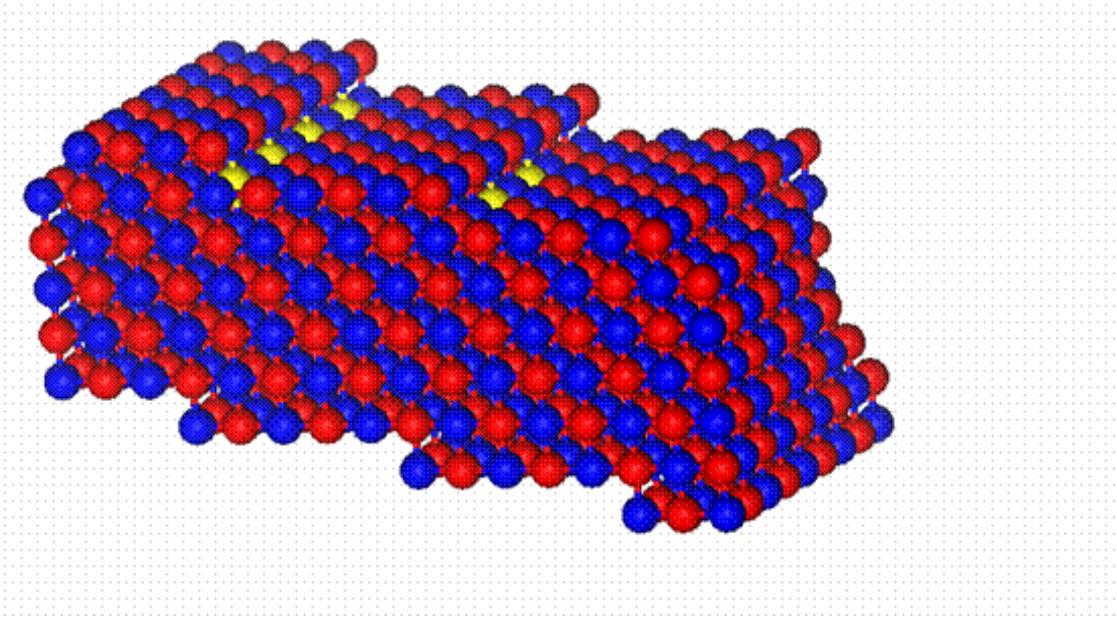

Figure 4.5: The CaO (510) surface layers of CaO where S is doped at the valley positions

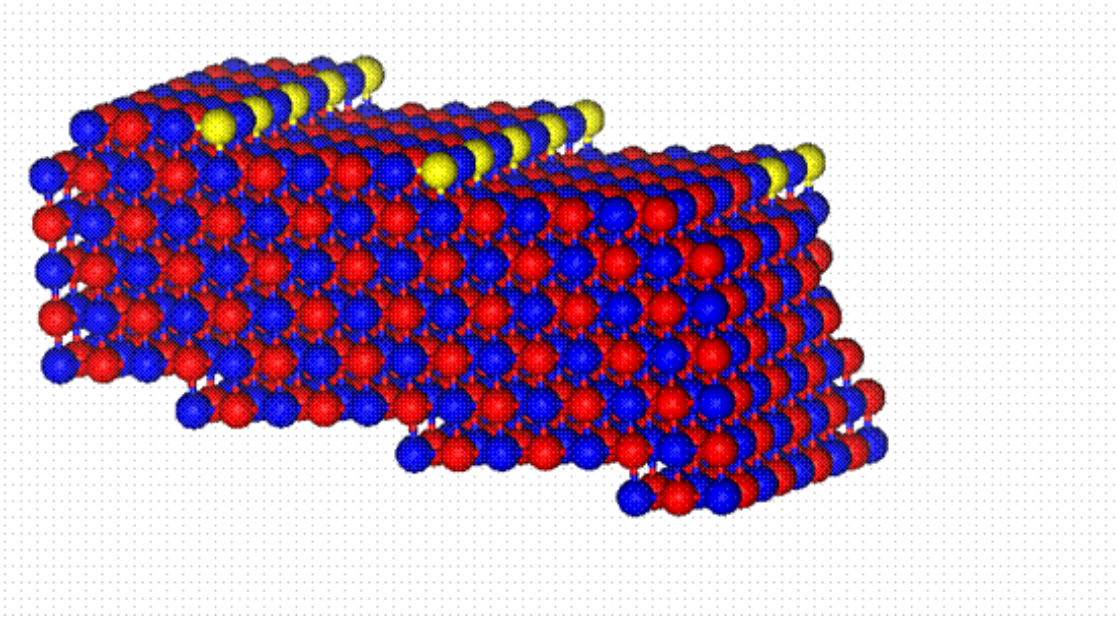

Figure 4.6: The CaO (510) surface layers of CaO where S is doped at the edge positions

in the valley position, up to 50%; at 62.5% the surface collapses. As in both CaS (110) and CaO (110) surface layers, the stability became more favoured on the valley than on the edge CaO (510) and CaS (510) calculated surfaces energies show the same trends as CaO (110) and CaS (110). The instability of the CaO (510) surface increases with sulphur coverage on both edges and valleys; where the edge doping is more favourable. On the contrary, the stability of CaS (510) is enhanced with increasing oxygen coverage at both edges and valleys. Beyond certain coverage, the surface energies become negative, implying that the surface collapses as additional oxygen atoms are introduced to the slab. The blank space in Table 4.3 and Table 4.5 on the CaS (110) and CaS (510) shows that the calculations exploded, consequently we don't have calculated surface energies.

4.8 Summary

In this chapter, we have shown how the migration of atoms in a crystal is calculated using Mott-Littleton method. Atoms move from lattice a position via the chosen interstitial path to another. The activation energies were determined and trends were compared with similar study where the molecules diffuse in crystal material. The defect energy calculations were also carried out, including Schottky and Frenkel defects. We have studied introduction of S and O on the CaO (100) and CaS (100) surfaces respectively. It was noted that these stable surfaces collapse as the percentage coverage of atoms increases. Surface energies, where S and O were located at

edges and valleys on both (110) and (510) surfaces of CaO and CaS, were calculated and depicted trends of stability. Studies of CaO (111) and CaS (111) with increasing S and O coverage respectively have also been carried out.

Chapter 5
Surface studies of CaO and CaS by Density Functional Theory

In this chapter we will discuss the adsorption of the molecules, H_2O, H_2S, HS and S_2 on the CaS (100) and CaO (100) surfaces, studied by the DFT method (CASTEP code). Only H_2O will be adsorbed on the 2x2 and 1x1 unit cell surfaces and other molecules will be adsorbed on the 1x1 surfaces of both CaS and CaO systems. The adsorption energies associated with different coverages of the molecules will be calculated.

5.1 Adsorption of the molecules on CaO (100) and CaS (100) surface slabs

5.1.1 Water molecule on the CaO (100) surface

Table 5.1 gives the adsorption energy of various molecules that are attached to the CaO surfaces. On the CaO (100) surface, H_2O molecules are likely to be intact, and are attached to the monolayer as indicated in Figure 5.1. The calculated adsorption energies at 25 %, 50 % , 75 % and 100 % coverages are -37.1 kJ/mol, -57.9 kJ/mol -58.0 kJ/mol and -59.5 kJ/mol respectively. Hence at 25 % coverage H_2O is least adsorbed as compared to 50 % to 100 % coverages and the latter are very close to each other. The adsorption energy results give similar trends as those of other DFT

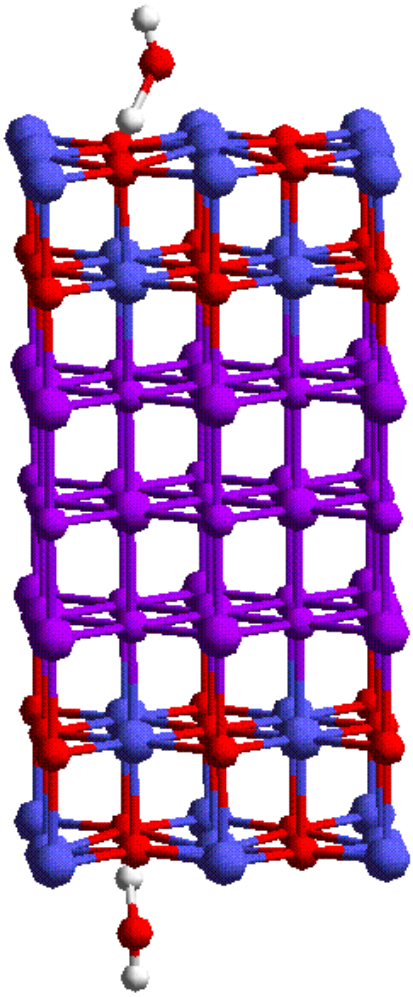

Figure 5.1: CaO (100) surface with 25% of H_2O attached on both surfaces.

methods [44], as demonstrated by -69.9 kJ/mol and -71.5 kJ/mol for 50 % and 100 % coverage respectively.

As shown in figure 5.1, the H_2O molecules are located at the surface slabs. The 25% coverage corresponds to one molecule attached to the surface. The distance from oxygen of CaO surface to hydrogen of the H_2O molecule is 1.043 Å . In the case of 50 % coverage, two molecules are attached to the slab and the distances between oxygen of CaO and hydrogen of H_2O ranges from 1.051 Å and 1.078 Å. For 75 % coverage, three molecules are located on the surfaces and the adsorption energy is -58.0 kJ/mol and the distance of the nearest oxygen atoms on the top layer and the H_2O molecules distances are 1.042 Å, 1.122Å and 1.137Å. In all coverages, we used the 2x2 supercell for calculations of adsorption energies, except for the 100 % coverage where the 1x1 surface was invoked. The latter coverage is made of one molecule attached to each side of the surface slab. The adsorption energy of this coverage is -59.8 kJ/mol and the nearest distance of the oxygen of CaO and hydrogen of the H_2O molecule was calculated as 1.465 Å. The short distance shows that H_2O molecules prefer to interact strongly with the surface. The attachment of the molecule on surfaces, also has an impact on other layers below the surface. The distance between oxygen and calcium, after relaxation, changed from 2.371 Å to 2.368 Å and from 2.409 Å to 2.270 Å.

5.1.2 H_2O molecule on the CaS (100) surface

The calculated adsorption energies of H_2O molecules on CaS are -44.4, -30.1, -47.4 and -47.4 kJ/mol for 25%, 50%, 75% and 100% coverages respectively, and do not reflect similar trends as those on the CaO surface (Table 5.1). The least adsorption of H_2O occurs at 50% coverage, unlike in CaO where it was noted at 25%. Similarities in CaO and CaS are observed at high coverages, i.e. 75 % and 100%, where adsorption appears to saturate. In the 25% coverage of CaS (100) surface, one H_2O molecule is attached to the each side of the slab. The distance between hydrogen of H_2O molecules and sulphur of CaS (100) surface on top layer is 2.277 Å At 50 % coverage, where two H_2O molecules are located on the surface slab, the nearest distances of hydrogen of H_2O molecule and sulphur of CaS (100) on the surface are 2.215 Å, 2.212 Å. 75% coverage is associated with three molecules attached to the top surface and the corresponding distances of H_2O molecules at 75% coverage are 2.370 Å, 2.189 Å, 2.218 Å. The 100 % coverage were done on 1x1 surface and its distance of hydrogen of H_2O molecule and sulphur of CaS (100) surfaces is 2.358 Å. There are currently no experimental results or previous calculations available to compare with our values for CaS.

5.1.3 Adsorption of H_2S, HS and S_2 on both CaO (100) and CaS (100) surface slabs

The adsorptions of all molecules mentioned in this section were simulated on the 1x1 surfaces of CaO (100) and CaS (100). Table 5.1 gives the adsorption energies

Surfaces	Molecules	Percentage coverage	Energy in kJ/mol
CaO	H_2O	25	-37.1
CaO	H_2O	50	-59.9
CaO	H_2O	75	-58.0
CaO	H_2O	100	-59.8
CaO	H_2S	100	-4.34
CaO	HS	100	-21.3
CaO	S_2	100	-113.0
CaS	H_2O	25	-44.4
CaS	H_2O	50	-30.1
CaS	H_2O	75	-47.4
CaS	H_2O	100	-47.4
CaS	H_2S	100	-141.0
CaS	HS	100	not properly converged
CaS	S_2	100	-127.0

Table 5.1: The adsorption energy of molecules attached on both (100) surface layers of CaO and CaS super cells.

for 100% coverage of H_2S, HS and S_2 on CaO (100) as -4.34, -21.3 and -113.0 kJ/mol respectively. It is apparent that S_2 is the most adsorbed molecule whilst H_2S is the least adsorbed. Reversed adsorption trends are reflected on the CaS (100) surface, where H_2S is the most adsorbed molecule (-141.0 kJ/mol) and S_2 is the least (-127.0 kJ/mol). The nearest distance of Ca on the CaO (100) surface and the S of S_2 molecule is 2.987 Å. In case of the H_2S adsorption on the CaO (100) surface, the nearest distance of S on the H_2S molecule and O in the top centre of CaO (100) surface is 1.05 Å. In comaparisson, H_2S on the CaS (100) surface, the nearest distance of hydrogen of H_2S molecule and S at the centre of the top layer of CaS (100) surface is 1.050 Å . The adsorption of S_2 on the CaS (100) surface resulted in the nearest distance from S of S_2 molecule and Ca of CaS (100) surface as 3.472 Å.

5.2 Summary

In this chapter we have considered the adsorption of molecules on the CaS (100) and CaO (100) surfaces. The adsorptions were done on 2x2 slab for H_2O molecules and 1x1 slab for all other molecules both CaS (100) and CaO (100) surfaces, which were helpful in varying surface coverage.

The adsorption results predict that H_2S is the least adsorbed molecules on CaO (100) surface and S_2 is most adsorbed. For CaS (100) surfaces H_2O is the least adsorbed on all coverages in comaparisson with all other mentioned molecules and

H_2S is most adsorbed. Note that HS is out of comparison since is not propertly converged.

Chapter 6
Conclusion

In the current study, atomistic simulations and DFT methods have been used to study defect and surface properties of CaO and CaS. Structural properties were calculated and converged surface energies determined the most stable surfaces, which also helped investigation of molecule adsorption on CaO and CaS systems. In atomistic simulations, region size variations were carried out for bulk systems in order to determine defect formation energies; and some of these defects are, vacancies, interstitials, impurities Schottky and Frenkel defects. The migrations paths of defects from one lattice position via interstitial path to the other vacant positions were established, and the activation energies of different types of defects were determined.

The contribution of O atoms on the CaS (100) surface and S on the CaO (100) surface were studied by atomistic simulations. The surface energy calculations indicated that the surface collapses as the coverage of the mentioned atoms is increased. The negative values show that the mentioned atoms prefer to be in the bulk than on the surfaces. In the case of CaO (110) and CaS (110) surfaces, an approach similar to that of (100) surfaces was followed. The surfaces on the edge are stable as compared to the surface energy on the valley. When we compare the overall surfaces energy calculations of (110) and (100) surfaces, the latter are more stable. Such a conclusion was reached by other previous calculations. It has further been shown that the for-

mation of CaS on top of the CaO surface (in atomistic calculations) is not favoured. CaO formation on the CaS surface is destabilizing the surface of CaS; as such the formation is favoured on the bulk than on the surfaces

The adsorption of molecules on both CaS (100) and CaO (100) surfaces were simulated at different surface coverages, using DFT calculations. A reduction of H_2O adsorption on the CaS (100) surface is noted from 25 to 50% coverage, which is followed by an increase and saturation between 75 and 100%. H_2O adsorption on the CaO (100) surface is enhanced from 25 to 50% and remains almost constant up to 100% coverage. In the case of the HS, H_2S and S_2 molecules, all calculations were carried out at 100 % coverage on CaO (100) and CaS (100) surfaces. S_2 and H_2S are respectively the most and least adsorbed molecules on CaO (100) surface. With converged results, the H_2S is the most adsorbed molecule on the CaS surface. It is recommended that adsorption experiments be conducted on surfaces of CaO and CaS, which will be useful for validating our predictions.

Appendix A

Presented papers at the conferences

M.J Ramusi and P.E Ngoepe , "Computational studies of electronic and structural properties of the first principle studies of CaO surfaces", presented at South African Institute of Physics (SAIP) 24 -27 September 2002 held at Potchefstroom University.

M.J Ramusi and P.E Ngoepe , "Computational studies of structural properties of CaO and CaS" presented at South African Institute of Physics (SAIP) 30 June 2004 held at the University of Free State.

M.J Ramusi and P.E Ngoepe , "Computational studies of structural properties of CaO and CaS" presented at Material Modelling Meeting (MMM) 31 March 2004 at University of Limpopo (Turloop Campus).

Bibliography

[1] P. Liu, T Kendelewicz, E. Nelson, G. A. Parks and G. E. Brown Jr., SSRL Activity Report 1997

[2] R.H Borgwardt and N. F. Roache, Ind. Eng. Chem. Proceess Des. Dev. 23, 742 (1984)

[3] R.H Borgwardt, Ind. Eng. Chem. Res. 28, 493 (1989)

[4] N.H. de Leeuw, G. W. Watson and S.C. Parker. J. Phys. Chem. 17219 (1995)

[5] Byoung-youl Coh, Kyu-Ho Cho and Ho-In Lee, J. Chem. Eng. of Japan, 34,138 (2001)

[6] http://www.shodor.org/chemviz/overview/compsci.html

[7] A. Al-Shawabkeh, H. Matsuda and M. Hasatani, Energy Convers. Mgmt, 38, 1389 (1997)

[8] V. L. Boris , K. Leonid, Polzik, L. Valary and Ugolkov, Thermochimica Act 390, 5 (2002)

[9] Z. Zeng and K. Natesan, fusion Eng. Des. 70 87 (2004)

[10] C.M. Mi, G.S. Cao, X.B. Zhao, Mat. Lett. 59, 127 (2005)

[11] H. Wajahat, Mirza and Soliman, I Al-Noury; Inter. J. of Cement Composites and Lightweight Concrete, 8, 81 (1986)

[12] H. L. Wang, M.J. Hedley and N.S Bolan, New Zealand J. of Agricultural Reseach, 38, 249 (1995)

[13] Cheng Chang and Peter, W. Swaan, Euro.J. Pharm.Sci., (2005)

[14] http://www.accelrys.com/technology/qm/erich/choice/html

[15] B. Szafran, S. Bednarek, J. Adamowski1, M.B. Tavernier, E. Anisimovas and F.M. Peeters, Eur. Phys. J. D 28, 373 (2004)

[16] H. M Evejen, Phys. Rev., 39, 675 (1932)

[17] P. P. Ewald, Ann. Phys., 64, 253 (1921)

[18] M.P. Tosi, Solid State Phys., 16, 1 (1964)

[19] R.A. Jackson and C. R. A. Catlow, Mol. Simul., 1, 207 (1999)

[20] U. Essmann, L. Perera, M. L. Berkowitz, T. Darden, H. Lee, and L. G. Pedersen, J. Chem. Phys., 101, 8870 (1994).

[21] L. Greengard and V. Rokhlin, J. Comput. Phys., 73, 325 (1987).

[22] S.W. de Leeuw, J.W. Perram, and E.R Smith, Proc. R. Soc. London, Ser. A, 373, 27 (1980).

[23] M. Leslie and M. J. Gillan, J. Phys. C, Solid State Phys., 18, 973 (1985).

[24] Lennard-Jones, J. E. Cohesion. Proceedings of the Physical Society ,43, 461 (1931).

[25] B. G. Dick, Jr.* and A. W. Overhauser, Phys. Rev. 112, 90 (1958)

[26] http://abulafia.mt.ic.ac.uk/publications/theses/stanek/methodology.pdf

[27] T. Grey, J. Gale, D. Nicholson and B. Peterson, Microporous and Mesoporous Materials, 31, 45 (1999)

[28] F. Mott and M. J. Littleton, Trans. Faraday Soc. 34, 485 (1938).

[29] D.R Hartree, proc. Camb. Phil. Soc. 24, 89 (1928).

[30] E. Schrodinger, Ann. Physik, 79, 361 (1926).

[31] C. Lee, N. Yang and R. G. Parr, Phys. Rev., B37, 785 (1988).

[32] W. Kohn, P. Vashishta, ‘Theory of the inhomogenous electron gas’, ed. S. Lundquist, N. H. Marck (New York, Plenum) (1983).

[33] W. Kohn and L. J. Sham, Phys. Rev 140, A1133 (1965).

[34] K. Ohno, K. Esfarjani, and Y. Kawazoe, Comp. Mat. Sci. (Springer, Berlin, 1999).

[35] D. C. Langreth and J. P. Perdew, Phys. Rev. B 21, 5469 (1980).

[36] D. Gay and A. Rohl, J. Chem. Soc. Faraday Trans. 91, 925 (1995).

[37] R. M. Dreizler and E. K. U. Gross, Density Functional Theory, (Springer, Berlin, 1990).

[38] E. Engel, in: Relativistic Electronic Structure Theory, Part 1. Fundamentals, edited by P. Schwerdtfeger, 524 (Elsevier, Amsterdam, 2002)

[39] E. K. U. Gross, J. F. Dobson, and M. Petersilka, Top. Curr. Chem. 181, 81 (1996).

[40] C. Speicher, R. M. Dreizler, and E. Engel, Ann. Phys. 213, 312 (1992).

[41] E. Wimmer, Mat. Scie. Eng., B37 72 (1996)

[42] J. P. McNamara, M. Sundararajan and I. H. Hillier, Journal of Molecular Graphics and Modelling, 24, 128 (2005)

[43] James O'keeffe, Chengyu Wei, Kyeongjae Cho, Appl. Phys. lett., 80, 676 (2002)

[44] N.H. de Leeuw, J.A. Purton, S.C. Parker, G.W. Watson and G. Kresse. Surf. Science 452, 9 (2000)

[45] T. J. Watson-Yang A. J. Freeman and D. D. Koelling, J.of Magn. Magn. Mat., 5, 277 (1977)

[46] J.C. Phillips, Phys. Rev. 112, 685 (1958).

[47] M. L. Cohen and V. Heine, Solid State Phys. 24, 37 (1970).

[48] M. C. Payne, M. P. Teter, D. C. Allan, and J. D. Joannopoulos, Rev. Mod. Phys, 64, 1045 (1992) .

[49] G. B. Bachelet, D. R. Hamann, and M. Schlüter, Phys. Rev. B 26, 4199 (1982).

[50] R. Car and M. Parrinello, Phys. Rev. Lett. 55, 2471 (1985).

[51] In Yong Kang, Yoon-Suk Kim, Yong-Chung, Hanchul Kim, Drek-Soo Kim and Jay J. Kim, Jounal of Ceramic Processing Reasech. 3, 171 (2002)

[52] V. Milman, B. Winkler, J. A. White, C. J. Pickard, M. C. Payne, E. V. Akhmatskaya, R. H. Nobes, Int. J. Quant. Chem. 77, 895 (2000)

[53] GULP - a computer program for the symmetry adapted simulation of solids, J.D. Gale, JCS Faraday Trans., 93, 629 (1997)

[54] A. Grzechnik and P Simon, J. Phys.: Condens. Matter 11, 2337 (1999)

[55] Sicence W. Y. Ching, Fangi Gan, and Ming-Zhu Huang, Phys. Rev. B 52, 1596 (1995).

[56] H. Baltache, R. Khenata, M. Sahnoun, M Driz, B. Abbar, B. Bouhafs, Physica B 344, 334 (2004)

[57] J. Sternerland and P.G Jonsson, ISIJ Intenational, 43, 26 (2003)

[58] P.J.H. van Beukering and M. A. Janssen, Resources , Concervation and Recycling, 33, 235 (2001)

[59] M.P Allen, D.J Tildesley, Phys. Rev. Lett. 78, 1291 (1997

[60] W.F van Gusteren, and P.K Weiner, Computational simulation of biomolecular system, ESCOM, Leiden (1989).

[61] N. L. Allinger, Y. H. Yuh, J.H. Lii, J. Am .Chem. Soc. 111, 8551 (1989).

[62] J. Maple, J., U. Dinur, A. T. Hagler, Proc. Nat. Acad. Sci. USA 85, 5350 (1998)

[63] C. R. A. Catlow and A. N. Cormack, Int. Rev. Phys. Chem. 6, 227 (1987).

[64] K. S. Kim, M. A. Moller, D. J. Tildesley, and N, Quirke, Mol. Sim. 13, 77 (1994).

[65] C. R. A. Catlow and J. M. Thomas, Phil. Trans. R. Soc. Lond. A 341, 255 (1992).

[66] P. Cortona and PMasri, J.Phys.,Condens. Matter, 10, 8947 (1998)

[67] P. Cortona and P. Masri, J. Phys. Condens. Matter, 10, 8945 (1998)

[68] T. Yamamoto, T. Litaka, R. Morishita and T. Ebisuzaki, RIKEN Review, No. 29 (June 2000)

[69] G.V Lewis and C.R.A Catlow, J Phys. C: Solid State Phys.,18, 1149 (1985)

[70] H.J Mankhorst and J.D Pack, Phys. Rev. B13, 5188 (1976)